Explicit Energy-Minimal Short-Term Path Planning for Collision Avoidance in Bidirectional Crowd Simulation

Mr. Saran Sillapaphiromsuk

จุฬาลงกรณ์มหาวิทยาลัย
CHULALONGKORN UNIVERSITY

A Dissertation Submitted in Partial Fulfillment of the Requirements
for the Degree of Doctor of Philosophy (Computer Engineering) in Computer Engineering
Department of Computer Engineering
Faculty of Engineering
Chulalongkorn University
Academic Year 2018
Copyright of Chulalongkorn University

การหาเส้นทางการเดินในระยะสั้นที่มีประสิทธิภาพบนพื้นฐานทางชีวกลศาสตร์ของการเดิน สำหรับการหลบหลีกในฝูงชนแบบสองทิศทาง

นายศรัณย์ ศิลปภิรมย์สุข

จุฬาลงกรณ์มหาวิทยาลัย
Chulalongkorn University

วิทยานิพนธ์นี้เป็นส่วนหนึ่งของการศึกษาตามหลักสูตรปริญญาวิศวกรรมศาสตรดุษฎีบัณฑิต
สาขาวิชาวิศวกรรมคอมพิวเตอร์ ภาควิชาวิศวกรรมคอมพิวเตอร์
คณะวิศวกรรมศาสตร์ จุฬาลงกรณ์มหาวิทยาลัย
ปีการศึกษา 2561

ลิขสิทธิ์ของจุฬาลงกรณ์มหาวิทยาลัย

Dissertation Title	Explicit Energy-Minimal Short-Term Path Planning for Collision Avoidance in Bidirectional Crowd Simulation
By	Mr. Saran Sillapaphiromsuk
Field of Study	Computer Engineering
Thesis Advisor	Assistant Professor Dr. Pizzanu Kanongchaiyos

Accepted by the Faculty of Engineering, Chulalongkorn University in Partial Fulfillment of the Requirement for the Doctor of Philosophy (Computer Engineering)

..... Dean of the Faculty of Engineering
(Associate Professor Supot Teachavorasinskun)

DISSERTATION COMMITTEE

..... Chairman
(Professor Dr. Prabhas Chongstitvatana)

..... Advisor
(Assistant Professor Dr. Pizzanu Kanongchaiyos)

..... External Examiner
(Dr. Pongsagon Vichitvejpaisal)

..... External Examiner
(Associate Professor Dr. Natasha Dejdumrong)

..... External Examiner
(Associate Professor Pavadee Sompagdee)

จุฬาลงกรณ์มหาวิทยาลัย
CHULALONGKORN UNIVERSITY

ศรัณย์ ศิลปภิรมย์สุข : การหาเส้นทางการเดินในระยะสั้นที่มีประสิทธิภาพบนพื้นฐานทางชีวกลศาสตร์ของการเดิน สำหรับการหลบหลีกในฝูงชนแบบสองทิศทาง. (Explicit Energy-Minimal Short-Term Path Planning for Collision Avoidance in Bidirectional Crowd Simulation) อ.ที่ปรึกษาหลัก : ผศ. ดร.พิษณุ คนองชัยยศ

การหาเส้นทางการเดินในระยะยาวรวมกับการหลบหลีกสิ่งกีดขวางรอบๆ เป็นวิธีทั่วไปที่ถูกนำมาใช้ในการจำลองการเคลื่อนไหวของตัวตนจำลองจากตำแหน่งหนึ่งไปยังอีกตำแหน่งหนึ่งโดยไม่ให้เกิดการชนกันระหว่างตัวตนจำลองกับวัตถุในฉากและระหว่างตัวตนจำลองด้วยกันเอง วิธีนี้สามารถให้ผลการจำลองที่ดีในสถานการณ์ที่ผู้คนสามารถเดินได้หลายทิศทาง แต่ในสถานการณ์ที่ผู้คนถูกจำกัดทิศทางการเดินให้เหลือเพียงหนึ่งหรือสองทิศทางนั้น ปรากฏว่าตัวตนจำลองมีลักษณะการเดินที่ผิดธรรมชาติ เช่น เดินเข้าไปติดและอยู่นิ่งระหว่างตัวตนจำลองสองตัวที่เดินสวนมาหรือเดินเข้าไปในพื้นที่ที่แออัดหรือมีกลุ่มคนเยอะๆ ทั้งๆที่ยังมีเส้นทางเดินที่ทำให้ตัวตนจำลองสามารถเดินหลบหลีกไปได้ ลักษณะเช่นนี้เกิดขึ้นบ่อยและเห็นได้ชัดในสถานการณ์แบบสองทิศทาง งานวิจัยนี้จึงได้เสนอขั้นตอนในการหาเส้นทางในระยะสั้นเพื่อขจัดความบกพร่องของพฤติกรรมการเดินของตัวตนจำลองในสถานการณ์แบบสองทิศทางนี้ขึ้น โดยใช้สมการพลังงานทางชีวกลศาสตร์ของการเดินเข้ามาเป็นตัวแปรที่บังคับให้ตัวตนจำลองมีความฉลาดในการเลือกเส้นทางในระยะสั้นได้ ผลลัพธ์ของการวิเคราะห์สมการพลังงานนั้น ช่วยบ่งบอกลักษณะของการเลือกเส้นทางการเดินที่ดีที่สุด โดยคำนึงถึงความเร็วที่ใช้เพื่อให้ประหยัดพลังงานที่สุด พร้อมๆ กับถึงจุดหมายปลายทางให้เร็วที่สุดด้วย นอกจากนี้ยังพบว่าการนำวิธีที่เสนอนี้ไปใช้ในสถานการณ์แบบหลายทิศทางนั้น ตัวตนจำลองสามารถหาเส้นทางที่เหมาะสมกว่าเมื่อเทียบกับวิธีก่อนอีกด้วย ยกตัวอย่าง เช่น ตัวตนจำลองสามารถเดินแทรกเข้าไปในช่องแคบๆ ของขบวนพาเหรดได้ เป็นต้น

สาขาวิชา	วิศวกรรมคอมพิวเตอร์	ลายมือชื่อนิสิต .....
ปีการศึกษา	2561	ลายมือชื่อ อ.ที่ปรึกษาหลัก .....

5471452421 : MAJOR COMPUTER ENGINEERING

KEYWORD: CROWD SIMULATION, BIDIRECTIONAL FLOW, PATH PLANNING, METABOLIC ENERGY

Saran Sillapaphiromsuk : Explicit Energy-Minimal Short-Term Path Planning for Collision Avoidance in Bidirectional Crowd Simulation. Advisor: Asst. Prof. Dr. Pizzanu Kanongchaiyos

In traditional crowd simulation, global path planning (GPP) and local collision avoidance (LCA) have been used to advance pedestrians toward their own goals without colliding. However, we found that using those methods in bidirectional flow can force a pedestrian to get stuck among the incoming people, walk through the congestion, and unintentionally occupy in a dense area, although more comfortable passageways are available. These behaviors are usually produced and simply noticeable. For this reason, the explicit metabolic-energy-minimal short-term path planning (MEM) is proposed and added between GPP and LCA to achieve more behavioral fidelity. For energy analysis, the optimal control theory with the objective energy function from the study of biomechanics is employed and finally leads to the very useful optimal walking characteristics for pedestrians. The simulation results show that the pedestrians with MEM can adapt their moving to avoid the congestion, resulting in more promising lane changing and overtaking behaviors. Even though MEM is mainly developed to deal with the artifacts in bidirectional flows, it can be extended with a little modification and produce significant behavioral improvement in multi-directional case.

Field of Study:	Computer Engineering	Student's Signature .....
Academic Year:	2018	Advisor's Signature .....

ACKNOWLEDGEMENTS

This dissertation would not have been completed without the help of many people to whom I am forever indebted.

First and foremost, I would like to express my deepest gratitude to my advisor, Dr. Pizzanu Kanongchaiyos, who provided invaluable guidance and assistance throughout my time as a student at Chulalongkorn University. Dr. Pizzanu Kanongchaiyos also inspire me to be a highly-passionate person about the methodologies behind computer graphics and computer vision. During being his advisee, I acquired so much knowledge from studying intensively on many topics in different areas of computer graphics research, and this would not have happened without his consent.

During my time at Chulalongkorn University, I have been very fortunate to enjoy the advise, support, and encouragement of my friends and colleagues in Computer Graphics Laboratory. Thank you!

Finally, I would like to thank my father and mother who always believed in me. I could not have done it without their support.

Saran Sillapaphiromsuk

จุฬาลงกรณ์มหาวิทยาลัย
CHULALONGKORN UNIVERSITY

TABLE OF CONTENTS

Page

..... iii

ABSTRACT (THAI) iii

..... iv

ABSTRACT (ENGLISH) iv

ACKNOWLEDGEMENTS v

TABLE OF CONTENTS vi

LIST OF FIGURES ix

CHAPTER 1 INTRODUCTION 1

1.1 Definition of Realistic Crowd Simulation 2

1.2 Problem, Scope, and Assumption 2

1.3 Contribution 3

1.4 Dissertation Organization 4

CHAPTER 2 PREVIOUS WORK 5

2.1 Global Path Planning 5

2.2 Local Collision Avoidance 6

2.2.1 Cellular Automata and Lattice Gas Model 6

2.2.2 Force Based Method 6

2.2.3 Rule Based Method 7

2.2.4 Vision Based Method 7

2.2.5 Psychology Based Method 8

2.2.6 Local Field Based Method 8

จุฬาลงกรณ์มหาวิทยาลัย
Chulalongkorn University

2.2.7 Example Based Method 9

2.2.8 Geometry Based Method 9

2.3 Uni- and Bidirectional Crowd Flows 10

CHAPTER 3 RELATED THEORIES AND PRINCIPLES 13

3.1 Principle of Least Effort 13

3.2 Biomechanics of Gait 13

3.3 Optimal Control Theory 14

3.3.1 Optimization Problem 15

3.3.2 Necessary Conditions for Optimality 16

3.3.3 Sufficient Conditions for Optimality 28

3.4 Dynamic Programming 33

CHAPTER 4 METABOLIC-ENERGY-MINIMAL SHORT-TERM PATH PLANNING 34

4.1 Overview of Our Crowd Simulation System 34

4.2 Metabolic-Energy-Minimal Short-Term Path Planning (MEM) 35

4.3 Constrained Optimization Problem 37

4.4 Metabolic-Energy-Minimal Walking Characteristics 38

4.4.1 Result from Constrained Optimization Problem 39

4.4.2 Useful Walking Characteristics 43

4.5 Near-Global Optimal Solution 46

4.6 Line Segment Pruning 50

4.7 The constant $\mathbf{e_s}$, $\mathbf{e_w}$, and $\mathbf{t}_{max}$ 50

CHAPTER 5 RESULTS AND DISCUSSION 52

5.1 Lane Changing and Overtaking Behavior 52

5.2 Mimicking the Real-World Bidirectional Flow 56

จุฬาลงกรณ์มหาวิทยาลัย
CHULALONGKORN UNIVERSITY

5.3 Lane Formation 56

5.4 Fundamental Diagrams of Traffic Flow 58

5.5 Computation Time 60

5.6 Multi-Directional Crowd Flow 62

CHAPTER 6 CONCLUSION AND FUTURE WORK 65

REFERENCES 66

VITA 73

จุฬาลงกรณ์มหาวิทยาลัย
CHULALONGKORN UNIVERSITY

LIST OF FIGURES

Page

Figure 1. Simulation result generated by our approach. The red-colored pedestrian walks through the huge crowd split by a bent, narrow passageway. At each time step, he observes his surroundings and chooses a comfortable way allowing him to reach to the front area. 11

Figure 2. The red pedestrian, who is located at the origin of the reference frame, is desired to walk toward the front line, or the red dashed line, with the lowest walking energy expenditure 35

Figure 3. Graphical meaning of the inequality constraint $w_j(\vec{p}(t),t) \leq 0$ used in our optimization problem. Suppose at a certain time t the optimal point $\vec{p}^{\,*}(t)$ on the optimal trajectory makes the constraint w_j active as shown in the figure, we can conclude that $\partial w_j^* / \partial \vec{p} \cdot \Delta\vec{p} \leq 0$ holds for every neighborhood $\vec{p}(t)$, when the distance between those two points ($\Delta\vec{p}$) is infinitesimal. 41

Figure 4. Graphical meaning of the endpoint constraint $f(\vec{p}(t_1)) = 0$. Since the endpoints of the optimal trajectory and the neighborhood must lie on this curve, so we can conclude that $(\partial f^* / \partial \vec{p})|_{t=t_1} \cdot \delta\vec{p}_1 = 0$ holds for every neighborhood of the optimal point $\vec{p}^{\,*}(t_1)$, when $\delta\vec{p}_1$ is infinitesimal. 42

Figure 5. Representation of perceived people. (a) The jth perceived people is represented by the circle equation w_j. (b) The approximation of w_j 47

Figure 6. Near-global energy-minimal velocity. (a) Pedestrian i perceived two people in front. The future position of the outside-l_{th}-zone pedestrian is predicted by extrapolating its projected velocity and extrapolating the current velocity for the inside one. (b) Horizontal and vertical lines of each perceived people generate two perpendicular planar strips, and the front line f creates a plane in space-time coordinate system. (c) The sampling time and maximum time are defined to discretize the time axis into levels to construct critical points. (d) The energy-minimal

velocity is computed from $\vec{v}_i^*$ obtained by the dynamic programming technique with the knowledge of the energy-minimal walking characteristics. 48

Figure 7. First-scenario comparison between our method and the other traditional ones. 54

Figure 8. Second-scenario comparison between our method and the other traditional ones. 55

Figure 9. Mimicking the real-world bidirectional crowd flows. 57

Figure 10. Lane formation simulation from a group of approximately one hundred pedestrians at each one end of the 13-meter-width corridor. The simulated pedestrians are placed randomly in the group and prefer to walk to the opposite side at the desired speed 1.3 m/s. 58

Figure 11. The fundamental diagrams of bidirectional crowd flows generated by our approach. 59

Figure 12. The average computation time of our approach in three different setting at different population densities. 61

Figure 13. Image sequence (from top to bottom) of two red pedestrians walking upward against a flow of crowds by using our approach. The red pedestrians can walk through the flow via the two tunnels marked by the red-colored rectangles. 63

Figure 14. Comparison between our method and the other traditional ones in multi-directional crowd simulation. 64

จุฬาลงกรณ์มหาวิทยาลัย
CHULALONGKORN UNIVERSITY

CHAPTER 1
INTRODUCTION

A situation when people are incidentally in a specific environment for a certain time period is a common phenomenon in an everyday life but when consider their movements it turns out to be an extremely difficult issue to predict their exact trajectories. This is due to the fact that each individual has his or her own decision-making that is influenced not only by his or her own physical and psychological factors but also by ones of the neighbors. With this complication, many researchers have been attempting to find a way to realistically simulate the movement trajectories of the people that can be applied in applications such as game, film, and engineering simulation.

The characteristics of movement trajectories do not depend on only the physical and psychological factors of pedestrians but also (1) the types of crowd flow and (2) the types of nearby objects. Types of crowd flow can be classified into three categories: uni-, bi- and multi-directional flow. Uni-directional flow is the simplest situation that restricts pedestrians to walk inside a passageway with only one entrance and one exit, and pedestrians are allowed to walk only one direction. If pedestrians are allowed to walk freely in a passageway regardless of the definition of the entrance or exit at the endpoint of the passageway, it was called bi-directional flow. The pedestrians in these two types of flow will find a way to overtake the others in front and change his current position to the adjacent collision-free lane. More complication is raised in multi-directional flow where pedestrians can absolutely free to walk in the area and must avoid collision with the others from many directions.

The nearby objects in crowd simulation can be classified into two types: *static* and *dynamic* objects. Static object refers to an object that cannot be displaced by itself or others. Any object, including walkable pedestrians, that can be displaced

is called dynamic object. Pedestrian can easily adapt his movement trajectory to avoid collision against static objects by using the mechanism called the global path planning. Global path planning will offer collision-free paths from position to position in a virtual world. All dynamic objects including virtual pedestrians will be ignored. It is like when the reader wants to travel from home to somewhere, first of all is the known possible routes to that place, and this will be handled by global path planning. However, the global path planning only tells us about the routes, not how fast a pedestrian should use along such path. For dynamic objects, the collision-free routes will be provided by using a mechanism called local collision avoidance that analyzes the surroundings of pedestrian based on different heuristics and then offers a walking direction to the pedestrian. The offered walking direction must advance the pedestrian toward his destination position along the path provided by global path planning. These two mechanisms have been extensively used in traditional crowd simulation.

1.1 Definition of Realistic Crowd Simulation

The interesting question is what is the definition of the word realistic in crowd simulation? The simplest answer is everything that can make virtual pedestrians look natural and similar to the real world in both visual aspect and behaviors. In this dissertation, we concern the behaviors of their movement trajectories. These behaviors can be validated using two approaches: qualitative and quantitative measurement. Qualitative measurement will compare the generated crowd behaviors with the ones frequently perceived in the real world, for examples, the lane formation behavior must be generated in bi-directional flow. But quantitative measurement will convert the generated crowd behaviors into numbers and compare with ones in the real world, for examples, the rate of change of the speed, the crowd density, and the rate of crowd flow.

1.2 Problem, Scope, and Assumption

Utilizing the global path planning and the local collision avoidance works well in multi-directional crowd flow. It can generate the satisfying results on pedestrian movements. However, when applying to pedestrians in bi-directional case, the strange behaviors were simply and noticeably generated as follows:

- A pedestrian gets stuck in the approaching people.
- A pedestrian chooses the nonsense direction of overtaking.
- A pedestrian gets pushed from the people walking behind.

With these results, the authors attempt to find a new crowd simulation system that is capable of dealing with these strange behaviors. The scope of this dissertation is limited to the following:

- This dissertation considers the pedestrian movements in bi-directional flow.
- This dissertation defines the realistic crowd simulation as the movement trajectories that frequently perceived in the real world, not the visual aspect of pedestrians such as cloths, hair, or color skin.
- The maximum pedestrian density in our experiment is no more than 3.5 ppl/m^2 because in real life the overtaking behavior does not frequently occur at the density higher than 3.5 ppl/m^2.

จุฬาลงกรณ์มหาวิทยาลัย
CHULALONGKORN UNIVERSITY

Additionally, the authors assume the following:

- All pedestrians know the walking direction to the one end of a passageway and cannot change it on-the-fly.
- Each pedestrian has only one desired speed throughout the simulation time and is set when the simulation begins.
- Each pedestrian has a limited perception radius to see the others.

1.3 Contribution

In this dissertation, we propose a new mechanism called metabolic-energy-minimal short-term path planning (MEM) which can be seamlessly added in between the existing global path planners (GPP) and the local collision avoidance methods (LCA) without modification. Our MEM can leverage the fidelity of the crowd movement in bi-directional flow to the next level by allowing a pedestrian to be able to automatically adapt himself in both walking direction and speed, which results in promising overtaking and lane changing behaviors.

Specifically, our crowd simulation system will begin with the GPP to compute the collision-free paths among the static obstacles, then instead of directly doing the LCA like many other traditional crowd simulation systems, the MEM will be employed to find the best desired walking direction from the predicted walking paths of neighboring pedestrians. MEM does not consider only the current positions, but also the future. This prevents a pedestrian from the successive awkward motion. Finally, the LCA employs the best desired direction to find the actual walking direction on the condition that the collision with the others should not occur. All these three mechanisms will be processed successively in each frame of simulation, making a pedestrian towards the destination position.

1.4 Dissertation Organization

จุฬาลงกรณ์มหาวิทยาลัย
CHULALONGKORN UNIVERSITY

The remainder of the dissertation is organized as follows. The next chapter reviews the previous work and points to related theories and principles in Chapter 3. In Chapter 4, we give an overview of our crowd simulation system and also detail our proposed MEM. In Chapter 5, we demonstrate the simulation results and discuss the efficiency and impact of our system on bi-directional crowd flow by comparing with the previous methods, and also show the usage of our system on multi-directional crowd simulation. We summarize the dissertation and point out the future work in Chapter 6.

CHAPTER 2
PREVIOUS WORK

Computer-aided simulation of the creatures' behaviors dates back to the work of Reynolds [1] who proposed the model to simulate the movement of the flock of birds. Since then, crowd behaviors have been extensively studied by the researchers in different disciplines, and the plenty of approaches were then developed in an effort to imitate the pedestrian navigation, which will be briefly overviewed in this section.

2.1 Global Path Planning

Dealing with avoiding static obstacles has been much addressed in the robotics literatures where the robot is treated as an intelligent machine capable of sensing the surroundings and planning the collision-free trajectories. We refer the reader to the valuable book [2] for the literature review and the useful planning algorithms. Likewise, autonomous pedestrians need to recognize the simulated world, and plan for a route to the destination. The simple way is to discretize the simulated world into the single uniform grid and use the well-known A* search algorithm for pathfinding, but it is inefficient for a large-scale environment in terms of computation time and memory used, so the multi-resolution grids [3] and the hierarchical pathfinding [4, 5] were introduced to enrich the performance. Owing to the tradeoff between the level of discretization and the performance, using a set of connected graphs to represent the walkable regions is a good choice to compromise between both of them. Many researchers construct such graphs based on different approaches, including the randomized method [6], Delaunay triangulation [7] navigation graph [8], voronoi diagram [9, 10], and medial axis [11-15]. The graph-based path planners yield a small-sized search space but the queried path, if it exists, is not the shortest one as produced in the grid-based planners. Moreover, the graphs can store additional information of each walkable region, for example, the

จุฬาลงกรณ์มหาวิทยาลัย
Chulalongkorn University

crowd density [16], to be used as the heuristic value in the traditional graph search algorithms.

2.2 Local Collision Avoidance

Without neighboring people, an autonomous pedestrian will walk on a path from GPP, but if a pedestrian is surrounded by the others, the pedestrian needs to dodge to avoid the collision. There are many works that takes an interest in this problem and we can categorize them into eight methods:

2.2.1 Cellular Automata and Lattice Gas Model

In cellular automata [17, 18], the virtual world is discretized to a rectangular grid and each cell in the grid is fully occupied by a virtual pedestrian. All pedestrians will walk based on some specified mechanism, or rules.

Lattice gas model [19, 20] is similar to the cellular automata but instead of discretizing a virtual world into a rectangular grid, the lattice gas model discretizes into the uniform mesh. Each node of the mesh can be occupied by a pedestrian. If lattice gas model represents a virtual world as the rectangular uniform mesh, it is completely the same as the rectangular grid in the cellular automata.

These models are easily implemented to handle collision avoidance, but the generated crowd behaviors are unrealistic due to the occupation condition in the discretized grid or mesh.

2.2.2 Force Based Method

In this method [21-23], virtual pedestrians are evolved in time by forces based on the Newton's motion laws. There are two types of forces: repulsive and attractive forces. The repulsive forces are responsible for the collision avoidance, and

the attractive forces for pedestrian following and goal seeking. The advantage of the method is it is easy to implement and can inherently generate the pushing behavior due to the nature of force. Moreover, the force-based method also implicitly reflects the social psychology of the human.

By the Newton's motion laws, the magnitude of all forces must be determined to compute the resultant one. The challenge is how to get the suitable magnitude of forces to drive the virtual pedestrians through the environment. It is inevitable that the weights of all forces must be specified. If the weights are extremely large, the strange behaviors will be exhibited, for example, the oscillation of virtual pedestrians.

2.2.3 Rule Based Method

Virtual pedestrians walk based on a collection of predefined rules. This gives us a challenge to find the rules that enough for simulating realistic crowd. If there are a small number of rules, the unrealistic behaviors may emerge because the behaviors of the real human are too complicated to be represented by a few rules. The rule-based method [24-26] produces remarkable results in case of low-density crowds, but lack realism in high-density because of the ambiguity of the dominant rule selection.

จุฬาลงกรณ์มหาวิทยาลัย
CHULALONGKORN UNIVERSITY

2.2.4 Vision Based Method

Based on the real human perception, the vision-based method [27] mimics the visual perception, similar to what our eyes can see, to be used for the navigation of virtual pedestrians. Pedestrians will visually perceive their surroundings and then produce two-dimensional images that represent what they actually see. To efficiently make the images, the graphics processing unit (GPU) is necessary, but it comes with the problem of data transmission between the GPU and CPU, so this issue must be deliberately considered, especially in high-density crowd simulation, because it very

much affects the overall computation time of the simulation pipeline. Moreover, the perceived virtual pedestrians could be approximated by simple geometries to reduce the complexity of the image usage.

Importantly, mimicking the visual perception from the real human is a good concept but the concern in navigational mechanism still remains.

2.2.5 Psychology Based Method

This method [28] attempt to find the relationship between the human psychology and the pedestrian movements based on observations and studies. In particular, some researchers [29] conduct the experiment to obtain the relation between psychological factors and the low-level walking parameters: the preferred speed, perceiving distance, the virtual pedestrian radius, maximum number of neighbors to be perceived, and the planning horizon, by asking the predefined questions involved with the human psychology to the volunteers and then finding the mathematical relation from the statistic answers.

The advantage of the psychology-based method is that the simulated pedestrians will exhibit the behaviors based on the real human psychology, but it is not trivial to conduct the procedure to obtain the real human psychological behaviors.

2.2.6 Local Field Based Method

Local-field based method constructs a field around a virtual pedestrian to be used as the area of perception. In this local field, there are many identical elements connected to each other and employed in a different way. Some researchers [30] define a local field as a uniform grid and then compute the desired velocities in all grid cells. Some researchers [31] define a local field as the connected circles with varying radii. Each circle contains the affordance values which provide the relative

strength of all possible steering decisions. Virtual pedestrian will walk on a path having the optimal affordance values.

The local field-based method reproduces not only the human perception but the short-range route finding as well. It comes with the idea that the real human rapidly plans the path to walk for the near future.

2.2.7 Example Based Method

To produce crowd behaviors as realistic as possible, the footages of the real human movements are provided in the example-based method [32-35]. The patterns of the real human movements are created as many as possible from the footages by either hand-selected or system-generated, and then collected in the database. In run-time phase, the desired velocity is obtained based on the matching function that maps the pattern of the virtual pedestrian to the real one in the database.

The advantage of the method is that the virtual pedestrians walk based on the walking patterns generated from the real human. The big challenges in the example-based method are finding the matching function, acquiring the number of the real human footages, and marking the walking patterns. Moreover, the more numbers of patterns created from the footages, the more realism of the virtual pedestrian movement, but the higher computation time when queries.

2.2.8 Geometry Based Method

Instead of computing the velocity from the Newton's motion laws in the force-based method, the geometry-based method [36, 37] directly computes the virtual pedestrian velocity based on the geometric appearances such as neighboring pedestrians' radii, positions, and velocities.

In addition, some researchers [38] aimed at constructing the region of admissible velocities, and proposed the technique called velocity obstacles, which is primarily used in the robotic research. Since the velocity obstacles method generates the oscillation motions, it is then enhanced and extensively used and applied to crowd simulation [39-46] eventually. Enhanced velocity obstacles method is simply implemented and exhibits collision-free, oscillation-free and smooth trajectories, and also offers parallel computing. Given the admissible velocity region, the challenge is how to choose the actual velocity from the region. The easiest way is choosing the velocity in the region that is closest to the desired velocity.

The other advantage of the geometry-based method is that the method does not require the weight tuning for odd behavior prevention, like the force-based method, since the geometry-based method directly chooses the velocity from the admissible region.

2.3 Uni- and Bidirectional Crowd Flows

In these situations, the GPP is easily defined due to the simplicity of static obstacle formation, which diverts the researcher interest to the local interaction between pedestrians. Some researchers simulate these circumstances using the lattice-gas model [19, 20] and cellular automata [47-49] with their own specific rules to determine the lane changing direction on a uniform grid. Although the rules were developed in different ways, the lane changing direction depends on the same attributes, including the crowd density and the walking directions of neighboring pedestrians being in frontal areas. Specifically, these rules will direct the pedestrians to walk on a more comfortable lane such as a low-density lane or a lane having the same-walking-direction pedestrians. By the nature of discretization, limiting pedestrian movement to a discrete set produces unrealistic results. Instead, the counterflow model [50] computes a new desired walking direction, based again on the crowd density and others' walking directions, enabling pedestrians in any continuous crowd simulators to walk toward a more comfortable area. Moreover, the overtaking

analysis based explicitly on the social repulsive forces [51, 52] allows pedestrians to weave their way through a crowd, but the repulsive forces may cancel each other, causing a pedestrian to get stuck into a moving group in front even though walkable pathways are available.

The above-mentioned works determine a new walking direction pointing to a more comfortable lane or area, by considering merely the current state of the neighboring. This does not guarantee the forthcoming movements, and often results in strange-looking behaviors, e.g., confronting the oncoming people, getting stuck into pedestrians in front, or unintentionally being in a dense area, even though other pathways exist. As we point out, the GPP and LCA do not consider the successive walking motion so the awkward behaviors are supposed to emerge. Recently, the navigational system called the Effective Avoidance Combination Strategy (EACS) [53] presented a mid-term motion planning technique, like our MEM, to compute an energy-efficient avoidance path made of successive adaptations. But their resulting path does not guarantee the minimal energy. It depends on the order of collision testing.

Figure 1. Simulation result generated by our approach. The red-colored pedestrian walks through the huge crowd split by a bent, narrow passageway. At each time step, he observes his surroundings and chooses a comfortable way allowing him to reach to the front area.

In our approach, the presence of MEM produces different behavioral results, comparing to the previous methods using only GPP and LCA. Because in GPP and

LCA no successive motions will be taken into account. Although some works exploit crowd density as a heuristic for guiding pedestrian walking, it is limited to some scenarios, for example, the scenario shown in Figure 1. Using crowd density for lane changing direction cannot guide the pedestrian to walk on a narrow passageway. Instead, pedestrians in our approach are guided by a collision-free path that yields the minimal energy. Our approach differs from EACS on the aspect that EACS may not consider some feasible paths because some orders of collision testing cannot be reachable, so some paths may be skipped. But in our approach the energy-minimal collision-free path is computed from all feasible paths which guarantees that the resulting path yields the global minimum energy.

จุฬาลงกรณ์มหาวิทยาลัย
CHULALONGKORN UNIVERSITY

CHAPTER 3
RELATED THEORIES AND PRINCIPLES

There are four principal subjects related in the research; first, the principle of least effort which reflects the psychological factors of the real human against actions, second, the biomechanics of gait which focuses on the walking mechanism of the real human, third, the optimal control theory which is essentially employed in order to mathematically model and analyze the research problem, and fourth, dynamic programming which is the important technique to reduce the complexity of problems by breaking them down into the simpler sub-problems.

3.1 Principle of Least Effort

The principle of least effort was studied by George K. Zipf [54], and states that it is a human nature to want the greatest outcome for the least amount of effort. This truly reflects the ordinary decision-making mechanism of the real human against actions to be performed. For example, the people frequently choose the shortest route when driving a car because it is highly inclined to yields the lowest amount of petrol. In the case of human walking, the people will frequently not choose a detour since it has a high tendency to make them more exhausted than the shortest one. This principle is abroad theory that covers many diverse fields involved with the human psychology against actions.

3.2 Biomechanics of Gait

The real human walking is a complex mechanism that we use in everyday life. Although it is a complex matter, we can easily distinguish the injured people from the normal ones through their walking motion. The biomechanics of gait [55] is the research area to study about the detailed mechanism behind the human walking in order to use in a clinically meaningful way.

จุฬาลงกรณ์มหาวิทยาลัย
Chulalongkorn University

Human walking mechanism is regulated by the coordination of the human limbs. Bone of each limb produces both kinetic energy and potential energy. To measure the efficiency of walking, kinetic energy and potential energy of every bone are computed and then summed up together, called the total mechanical energy. Since it is not trivial to compute the total mechanical energy at every time step to gain the human walking efficiency in a certain period of time, many researchers attempt to find a better indicator to measure the efficiency of walking. The experiment to measure the oxygen uptake is then well conducted. In the experiment, the subjects were required to breathe through a mouth piece, which is an oxygen uptake measuring instrument, while walking on a treadmill with different speeds. Finally, the relationship between the energy consumption and the speed of walking was obtained. This kind of energy is called the metabolic energy.

$$P = e_s + e_w \|v\|^2 \tag{3.1}$$

where P is the metabolic consumption power (J/kg.s), v is the velocity (m/s), e_s is the energy consumption coefficient when standing (J/kg.s), .and e_w is the energy consumption coefficient when walking (Js/kg.m^2).

For the average human, $e_s = 2.23$ and $e_w = 1.25$, and the most efficient walking speed of the average human that yields the lowest amount of metabolic consumption power is:

$$\|v\|_{eff} = \sqrt{\frac{e_s}{e_w}} = 1.34 \quad \text{m/s} \tag{3.2}$$

3.3 Optimal Control Theory

A problem we are dealing with in this dissertation is the optimization problem having the objective function in the integral form with N inequality constraints and

one free endpoint condition. This type of problem is a special case in the optimal control theory. For more detail and other cases of problem, we refer the reader to these optimal control theory books [56-58].

3.3.1 Optimization Problem

Our optimization problem begins with minimizing the objective function in the integral form as shown in the following equation:

$$E = \int_{t_0}^{t_1} g(t, \vec{p}(t), \vec{v}(t))dt, \tag{3.3}$$

where $\vec{p} \in \mathcal{R}^m$ and $\vec{v} \in \mathcal{R}^n$ are called the state and control variables, respectively, and $g(\cdot)$ is a real-valued function. When the values of the control variables $\vec{v}$ change, the values of the state variables $\vec{p}$ will be changed simultaneously by this differential equation:

$$\dot{\vec{p}}(t) = \vec{h}(t, \vec{p}(t), \vec{v}(t)), \tag{3.4}$$

where $\vec{h}(\cdot)$ is arbitrary vector function that has the same dimension as $\vec{p}$. The state $\vec{p}(t)$ is also constrained by the N inequality equations:

$$w_j(\vec{p}(t), t) \leq 0, \quad j = 1, \ldots, N. \tag{3.5}$$

for all $t \in [t_0, t_1]$, and one endpoint constraint:

$$f(\vec{p}(t_1)) = 0. \tag{3.6}$$

The function w_j and f are the real-valued functions. We assume that all functions are continuously differentiable with respect to their own independent arguments.

Notice that the control function $\vec{v}(t)$ influences the functional E directly by its own values and indirectly by its impact on the state function $\vec{p}(t)$ in Eq.(3.4). Moreover, in our problem, the initial point of the state $\vec{p}(t)$ is fixed in both space and time and can be computed in advance. That is:

t_0 and $\vec{p}(t_0)$ are fixed to the known values.

3.3.2 Necessary Conditions for Optimality

To find the optimal trajectory (t, $\vec{p}^{\,*}(t)$, $\vec{v}^{\,*}(t)$), we first eliminate Eq.(3.4) by appending it into the functional E with the Lagrange multiplier vector function $\vec{\lambda}(t)$, which results in:

$$E = \int_{t_0}^{t_1} g(t,\vec{p}(t),\vec{v}(t)) + \vec{\lambda}(t)\cdot\left[\vec{h}(t,\vec{p}(t),\vec{v}(t)) - \dot{\vec{p}}(t)\right]dt, \tag{3.7}$$

where the Lagrange multiplier $\vec{\lambda}(t) \in \mathcal{R}^m$ can be arbitrary vector function. Then, we expand the product term and apply the integration by parts, so Eq.(3.7) turns out to be:

$$E = \int_{t_0}^{t_1} \left[g + \vec{\lambda}\cdot\vec{h} + \dot{\vec{\lambda}}\cdot\vec{p} \right] dt + \vec{\lambda}(t_0)\cdot\vec{p}(t_0) - \vec{\lambda}(t_1)\cdot\vec{p}(t_1), \tag{3.8}$$

Note that we discard the arguments of the functions in the integral just because of the limited space and for the clear explanation. Please remember that such functions still depend on their own independent variables that are previously displayed. We assume that the optimal trajectory (t, $\vec{p}^{\,*}(t)$, $\vec{v}^{\,*}(t)$) over time period $[t_0, t_1]$ produces the minimum functional E^* within some neighborhoods E, so from Eq.(3.15) we obtain:

$$E^* = \int_{t_0}^{t_1} \left[g^* + \vec{\lambda} \cdot \vec{h}^* + \dot{\vec{\lambda}} \cdot \vec{p}^* \right] dt + \vec{\lambda}(t_0) \cdot \vec{p}^*(t_0) - \vec{\lambda}(t_1) \cdot \vec{p}^*(t_1), \quad (3.9)$$

where the asterisk in the superscript means the function is evaluated at the optimal trajectory $(t, \vec{p}^*(t), \vec{v}^*(t))$.

For the neighborhoods of $(t, \vec{p}^*(t), \vec{v}^*(t))$, if trajectories $(t, \vec{p}(t), \vec{v}(t))$ for $t \in [t_0, t_1 + \delta t_1]$ are its neighborhoods, they must produce higher or equal functional E to the minimum functional E^*. Note that the state at the endpoint in our case is free in both space and time, so the time of the endpoint of neighboring trajectories can be shifted and this is the reason why the upper bound must be $t_1 + \delta t_1$, where δt_1 is a small infinitesimal quantity. From Eq.(3.7), the functional E produced by the neighborhoods $(t, \vec{p}(t), \vec{v}(t))$ can be computed by:

$$E = \int_{t_0}^{t_1 + \delta t_1} \left[g + \vec{\lambda} \cdot \vec{h} - \vec{\lambda} \cdot \dot{\vec{p}} \right] dt. \quad (3.10)$$

จุฬาลงกรณ์มหาวิทยาลัย
CHULALONGKORN UNIVERSITY

Rewrite Eq.(3.10) by splitting the integral at time t_1 into two separate terms, so

$$E = \int_{t_0}^{t_1} \left[g + \vec{\lambda} \cdot \vec{h} - \vec{\lambda} \cdot \dot{\vec{p}} \right] dt + \int_{t_1}^{t_1 + \delta t_1} \left[g + \vec{\lambda} \cdot \vec{h} - \vec{\lambda} \cdot \dot{\vec{p}} \right] dt. \quad (3.11)$$

The first integral term on the right side of Eq.(3.10) is the same form as one in Eq.(3.7), so it can be replaced with the right side of Eq.(3.8). Therefore,

$$E = \int_{t_0}^{t_1} \left[g + \vec{\lambda} \cdot \vec{h} + \dot{\vec{\lambda}} \cdot \vec{p} \right] dt + \vec{\lambda}(t_0) \cdot \vec{p}(t_0) - \vec{\lambda}(t_1) \cdot \vec{p}(t_1) + \int_{t_1}^{t_1+\delta t_1} \left[g + \vec{\lambda} \cdot \vec{h} - \vec{\lambda} \cdot \dot{\vec{p}} \right] dt \tag{3.12}$$

Consider the last integral term in Eq.(3.12), it can be approximated by:

$$\begin{aligned} \int_{t_1}^{t_1+\delta t_1} \left[g + \vec{\lambda} \cdot \vec{h} - \vec{\lambda} \cdot \dot{\vec{p}} \right] dt &\approx \left[g + \vec{\lambda} \cdot \vec{h} - \vec{\lambda} \cdot \dot{\vec{p}} \right] \Big|_{t_1} \delta t_1 \\ &= g \big|_{t=t_1} \delta t_1 \\ &\approx \left[g^* + \frac{\partial g^*}{\partial \vec{p}} \cdot \Delta \vec{p} + \frac{\partial g^*}{\partial \vec{v}} \cdot \Delta \vec{v} + R_2^* \right] \Bigg|_{t=t_1} \delta t_1 \\ &\approx g^* \Big|_{t=t_1} \delta t_1 \end{aligned} \tag{3.13}$$

where $\Delta \vec{p}(t) = \vec{p}(t) - \vec{p}^*(t)$, $\Delta \vec{v}(t) = \vec{v}(t) - \vec{v}^*(t)$, and R_2^* is the remainder. The second line in Eq.(3.13) is from eliminating the last two terms from the first line. This was due to the equality constraint specified in Eq.(3.4). The third line results from applying the Taylor series expansion to the function g about the optimal trajectory $(t, \vec{p}^*(t), \vec{v}^*(t))$. The term $\Delta \vec{p} \delta t_1$, $\Delta \vec{v} \delta t_1$, and $R_2^* \delta t_1$ are very small, so they are eliminated, and finally we obtain its approximation shown in the last line. Therefore, Eq.(3.12) becomes:

$$E = \int_{t_0}^{t_1} \left[g + \vec{\lambda} \cdot \vec{h} + \dot{\vec{\lambda}} \cdot \vec{p} \right] dt + \vec{\lambda}(t_0) \cdot \vec{p}(t_0) - \vec{\lambda}(t_1) \cdot \vec{p}(t_1) + g^* \Big|_{t=t_1} \delta t_1 \tag{3.14}$$

Since the functional E^* is a local minima within some neighborhood E, which is expressed by Eq.(3.14), so we get

$$E - E^* \geq 0. \tag{3.15}$$

Consider $E - E^*$ from Eq.(3.9) and Eq.(3.14),

$$\begin{aligned} E - E^* \triangleq & \int_{t_0}^{t_1} \left[(g - g^*) + \vec{\lambda} \cdot (\vec{h} - \vec{h}^*) + \dot{\vec{\lambda}} \cdot (\vec{p} - \vec{p}^*) \right] dt \\ & + \vec{\lambda}(t_0) \cdot \left[\vec{p}(t_0) - \vec{p}^*(t_0) \right] - \vec{\lambda}(t_1) \cdot \left[\vec{p}(t_1) - \vec{p}^*(t_1) \right] \\ & + g^* \Big|_{t=t_1} \delta t_1 . \end{aligned}$$

Then, we use the Taylor series expansion on the terms $g - g^*$ and $\vec{h} - \vec{h}^*$, and change $\vec{p} - \vec{p}^*$ to $\Delta\vec{p}$.

$$\begin{aligned} E - E^* \triangleq & \int_{t_0}^{t_1} \left[\frac{\partial g^*}{\partial \vec{p}} \cdot \Delta\vec{p} + \frac{\partial g^*}{\partial \vec{v}} \cdot \Delta\vec{v} \right] dt \\ & + \int_{t_0}^{t_1} \left[\sum_{i=1}^{m} \lambda_i \left[\frac{\partial h_i^*}{\partial \vec{p}} \cdot \Delta\vec{p} + \frac{\partial h_i^*}{\partial \vec{v}} \cdot \Delta\vec{v} \right] + \dot{\vec{\lambda}} \cdot \Delta\vec{p} \right] dt \\ & + \vec{\lambda}(t_0) \cdot \Delta\vec{p}(t_0) - \vec{\lambda}(t_1) \cdot \Delta\vec{p}(t_1) + g^* \Big|_{t=t_1} \delta t_1 , \end{aligned} \tag{3.16}$$

where λ_i is the ith component of the Lagrange multiplier vector function $\vec{\lambda}$, and h_i is the ith component of the vector function $\vec{h}$. As the state at initial point, the state at time t_0, in our case is fixed in both space and time, so $\Delta\vec{p}(t_0) = 0$, and Eq.(3.16) becomes:

$$
\begin{aligned}
E - E^* \triangleq & \int_{t_0}^{t_1} \left[\frac{\partial g^*}{\partial \vec{p}} \cdot \Delta\vec{p} + \frac{\partial g^*}{\partial \vec{v}} \cdot \Delta\vec{v} \right] dt \\
& + \int_{t_0}^{t_1} \left[\sum_{i=1}^{m} \lambda_i \left[\frac{\partial h_i^*}{\partial \vec{p}} \cdot \Delta\vec{p} + \frac{\partial h_i^*}{\partial \vec{v}} \cdot \Delta\vec{v} \right] + \dot{\vec{\lambda}} \cdot \Delta\vec{p} \right] dt \\
& - \vec{\lambda}(t_1) \cdot \Delta\vec{p}(t_1) + g^* \Big|_{t=t_1} \delta t_1,
\end{aligned}
\tag{3.17}
$$

Let $\delta\vec{p}_1$ be the difference between the endpoint of the optimal state $\vec{p}^*$, which ends at the time t_1, and the endpoint of the neighborhood $\vec{p}$, which ends at the time $t_1 + \delta t_1$. Specifically, $\delta\vec{p}_1 = \vec{p}(t_1 + \delta t_1) - \vec{p}^*(t_1)$. So $\Delta\vec{p}(t_1)$ can be approximated by:

$$
\Delta\vec{p}(t_1) \approx \delta\vec{p}_1 - \dot{\vec{p}}^*(t_1)\delta t_1.. \tag{3.18}
$$

Replacing it in Eq.(3.17) results in:

$$
\begin{aligned}
E - E^* \triangleq & \int_{t_0}^{t_1} \left[\frac{\partial g^*}{\partial \vec{p}} \cdot \Delta\vec{p} + \frac{\partial g^*}{\partial \vec{v}} \cdot \Delta\vec{v} \right] dt \\
& + \int_{t_0}^{t_1} \left[\sum_{i=1}^{m} \lambda_i \left[\frac{\partial h_i^*}{\partial \vec{p}} \cdot \Delta\vec{p} + \frac{\partial h_i^*}{\partial \vec{v}} \cdot \Delta\vec{v} \right] + \dot{\vec{\lambda}} \cdot \Delta\vec{p} \right] dt \\
& + \left[g^* \Big|_{t=t_1} + \vec{\lambda}(t_1) \cdot \dot{\vec{p}}^*(t_1) \right] \delta t_1 - \vec{\lambda}(t_1) \cdot \delta\vec{p}_1.
\end{aligned}
\tag{3.19}
$$

Rearrange terms in the integrand in Eq.(3.19), so we get:

$$
\begin{aligned}
E - E^* \triangleq & \int_{t_0}^{t_1} \left[\frac{\partial g^*}{\partial \vec{p}} + \sum_{i=1}^{m} \lambda_i \frac{\partial h_i^*}{\partial \vec{p}} + \dot{\vec{\lambda}} \right] \cdot \Delta \vec{p} \; dt \\
& + \int_{t_0}^{t_1} \left[\frac{\partial g^*}{\partial \vec{v}} + \sum_{i=1}^{m} \lambda_i \frac{\partial h_i^*}{\partial \vec{v}} \right] \cdot \Delta \vec{v} \; dt \\
& + \left[g^* \Big|_{t=t_1} + \vec{\lambda}(t_1) \cdot \dot{\vec{p}}^*(t_1) \right] \delta t_1 - \vec{\lambda}(t_1) \cdot \delta \vec{p}_1 .
\end{aligned}
\tag{3.20}
$$

Let $\mathcal{H}(t, \vec{p}(t), \vec{v}(t), \vec{\lambda}(t)) = g + \vec{\lambda} \cdot \vec{h}$, which is called the Hamiltonian. So, Eq.(3.20) turns out to be:

$$
\begin{aligned}
E - E^* \triangleq & \int_{t_0}^{t_1} \left[\left[\frac{\partial \mathcal{H}^*}{\partial \vec{p}} + \dot{\vec{\lambda}} \right] \cdot \Delta \vec{p} + \frac{\partial \mathcal{H}^*}{\partial \vec{v}} \cdot \Delta \vec{v} \right] dt \\
& + \mathcal{H}^* \Big|_{t=t_1} \delta t_1 - \vec{\lambda}(t_1) \cdot \delta \vec{p}_1 .
\end{aligned}
\tag{3.21}
$$

From Eq.(3.15) and Eq.(3.21), the optimal trajectory $(t, \vec{p}^*, \vec{v}^*)$ which produces the local minimum functional E^* must satisfy the following equation:

$$
\begin{aligned}
\int_{t_0}^{t_1} & \left[\left[\frac{\partial \mathcal{H}^*}{\partial \vec{p}} + \dot{\vec{\lambda}} \right] \cdot \Delta \vec{p} + \frac{\partial \mathcal{H}^*}{\partial \vec{v}} \cdot \Delta \vec{v} \right] dt \\
& + \mathcal{H}^* \Big|_{t=t_1} \delta t_1 - \vec{\lambda}(t_1) \cdot \delta \vec{p}_1 \geq 0.
\end{aligned}
\tag{3.22}
$$

The optimal trajectory $(t, \vec{p}^*, \vec{v}^*)$ yields the local minimum E^* over *all* admissible neighborhoods $(t, \vec{p}, \vec{v})$, and *some* neighborhoods $(t, \vec{p}, \vec{v})$ could have the same endpoint in both space and time as the endpoint of the optimal trajectory $(t, \vec{p}^*, \vec{v}^*)$, that is $\delta t_1 = 0$ and $\delta \vec{p}_1 = 0$, which turns Eq.(3.22) into

$$\int_{t_0}^{t_1}\left[\left[\frac{\partial \mathcal{H}^*}{\partial \vec{p}}+\dot{\vec{\lambda}}\right]\cdot\Delta\vec{p}+\frac{\partial \mathcal{H}^*}{\partial \vec{v}}\cdot\Delta\vec{v}\right]dt \geq 0. \tag{3.23}$$

So the optimal trajectory $(t,\vec{p}^{\,*}(t),\vec{v}^{\,*}(t))$ must satisfy

$$\left[\frac{\partial \mathcal{H}^*}{\partial \vec{p}}+\dot{\vec{\lambda}}\right]\cdot\Delta\vec{p}+\frac{\partial \mathcal{H}^*}{\partial \vec{v}}\cdot\Delta\vec{v} \geq 0, \tag{3.24}$$

for all $t \in [t_0, t_1]$.

Back to the N inequality constraints in Eq.(3.5). We call the constraint w_j is *inactive* at time t, if $w_j(\vec{p}(t),t) < 0$; otherwise, *active* at time t. If the optimal state $\vec{p}^{\,*}(t)$ makes the *j*th constraint w_j inactive at a certain time t, so $w_j(\vec{p}^{\,*}(t),t) < 0$. However, for any neighborhood $\vec{p}(t)$, it must satisfy Eq.(3.5), so $w_j(\vec{p}(t),t) \leq 0$. This conduces to:

$$w_j(\vec{p}(t),t) \ \{>,=,\text{or} \ <\} \ w_j(\vec{p}^{\,*}(t),t)$$

which places no restriction on $\Delta\vec{p}(t)$. On the other hand, if the optimal state $\vec{p}^{\,*}(t)$ makes the *j*th constraint w_j active at a certain time t, so $w_j(\vec{p}^{\,*}(t),t) = 0$, and, as before, the neighborhood $\vec{p}(t)$ must satisfy $w_j(\vec{p}(t),t) \leq 0$. This conduces to:

$$w_j(\vec{p}(t),t) \ \leq \ w_j(\vec{p}^{\,*}(t),t)$$

and results in the restriction on $\Delta\vec{p}(t)$ as shown below:

$$\frac{\partial w_j^*}{\partial \vec{p}}\cdot\Delta\vec{p} \ \leq \ 0. \tag{3.25}$$

In case the optimal state $\vec{p}^{\,*}(t)$ makes *all* constraints w_j *inactive* at a certain time t, so $\Delta\vec{p}(t)$ will not be constrained by any w_j. This leads to any possibilities of values of $\Delta\vec{p}$ at time t. Likewise, the control $\vec{v}(t)$ is also arbitrary, leading to arbitrary $\Delta\vec{v}$ as well. Therefore, to satisfy Eq.(3.24) when $\Delta\vec{p}(t)$ and $\Delta\vec{v}(t)$ can be arbitrary, the terms in the parentheses must be zero:

$$\frac{\partial\mathcal{H}^*}{\partial\vec{p}} + \dot{\vec{\lambda}} = 0 \quad \text{and} \quad \frac{\partial\mathcal{H}^*}{\partial\vec{v}} = 0. \tag{3.26}$$

Eq.(3.26) expresses the characteristics of the optimal state $\vec{p}^{\,*}(t)$ and optimal control $\vec{v}^{\,*}(t)$ in a certain time period when all inequality constraints are inactive.

In case the optimal state $\vec{p}^{\,*}(t)$ makes *some/all* constraints w_j *active*. All active w_j must place the restriction on $\Delta\vec{p}(t)$, as shown in Eq.(3.25). So

$$\frac{\partial w_j^*}{\partial\vec{p}} \cdot \Delta\vec{p} \quad \leq \quad 0, \qquad j \in \mathcal{A}_t, \tag{3.27}$$

where $\mathcal{A}_t$ is a set of indices of the active constraints at time t. To satisfy Eq.(3.24) when $\Delta\vec{p}(t)$ is constrained by Eq.(3.27), the Farkas's lemma, described in the appendix, is then employed. This results in:

$$\frac{\partial\mathcal{H}^*}{\partial\vec{p}} + \dot{\vec{\lambda}} + \sum_{j\in\mathcal{A}_t} \alpha_j(t)\frac{\partial w_j^*}{\partial\vec{p}} = 0 \quad \text{and} \quad \frac{\partial\mathcal{H}^*}{\partial\vec{v}} = 0, \tag{3.28}$$

where $\alpha_j(t) \geq 0$ for all $j \in \mathcal{A}_t$. Eq.(3.28). expresses the characteristics of the optimal state $\vec{p}^{\,*}(t)$ and optimal control $\vec{v}^{\,*}(t)$ in a certain time period when some/all inequality constraints are active.

Notice from Eq.(3.26) and Eq.(3.28). that if an inequality constraint becomes active by the optimal state $\vec{p}^{\,*}$, the term $\alpha_j \partial w_j^{\,*} / \partial \vec{p}$ will be added. So, we generalize this by raising the additional equation shown below:

$$\alpha_j(t) w_j(\vec{p}^{\,*}(t), t) \;=\; 0, \qquad j = 1, \ldots, N.$$

In summary, the optimal trajectory $(t, \vec{p}^{\,*}(t), \vec{v}^{\,*}(t))$ must satisfy:

$$\begin{aligned} \dot{\vec{\lambda}} + \frac{\partial \mathcal{L}^*}{\partial \vec{p}} &= 0 \\ \frac{\partial \mathcal{L}^*}{\partial \vec{v}} &= 0 \\ \alpha_j(t) w_j(\vec{p}^{\,*}(t), t) &= 0, \qquad j = 1, \ldots, N \\ \alpha_j(t) &\geq 0, \qquad j = 1, \ldots, N \\ \vec{\lambda}(t) &\in \mathcal{R}^m, \end{aligned} \tag{3.29}$$

for all $t \in [t_0, t_1]$, where $\mathcal{L}$ is called the Lagrangian and equals to:

$$\mathcal{L}(t, \vec{p}(t), \vec{v}(t), \vec{\lambda}(t), \alpha_1(t), \ldots, \alpha_N(t)) = \mathcal{H} + \sum_{j=1}^{N} \alpha_j(t) w_j(\vec{p}(t), t)$$

So far we completely investigate the characteristics of the optimal trajectory $(t, \vec{p}^{\,*}, \vec{v}^{\,*})$ against the neighborhoods $(t, \vec{p}, \vec{v})$ that have the same endpoint in both space and time as one of the optimal trajectory. Now it is time to investigate the characteristics of the optimal trajectory $(t, \vec{p}^{\,*}, \vec{v}^{\,*})$ against the neighborhoods $(t, \vec{p}, \vec{v})$ that have different endpoint to one of the optimal trajectory. That is $\delta t_1 \neq 0$ and $\delta \vec{p}_1 \neq 0$. Do not forget that Eq.(3.22) must hold for the optimal

trajectory $(t, \vec{p}^{\,*}, \vec{v}^{\,*})$, and because Eq.(3.23) holds in the previous investigation, so Eq.(3.22) turns out to be:

$$\mathcal{H}^{*}\Big|_{t=t_1} \delta t_1 - \vec{\lambda}(t_1) \cdot \delta \vec{p}_1 \;\; \geq \;\; 0. \tag{3.30}$$

However, the endpoints are constrained by Eq.(3.6), which yields:

$$f(\vec{p}^{\,*}(t_1)) = 0 \quad \text{and} \quad f(\vec{p}(t_1 + \delta t_1)) = 0.$$

Recall that the optimal state $\vec{p}^{\,*}$ and the neighborhood $\vec{p}$ are assumed to end at the time t_1 and $t_1 + \delta t_1$, respectively. Because of $\vec{p}(t_1 + \delta t_1) = \vec{p}^{\,*}(t_1) + \delta \vec{p}_1$, so we get:

$$f(\vec{p}^{\,*}(t_1)) = 0 \quad \text{and} \quad f(\vec{p}^{\,*}(t_1) + \delta \vec{p}_1) = 0.$$

Using the Taylor series expansion to above equations yields the following constraint towards $\delta \vec{p}_1$:

$$\left[\frac{\partial f^{*}}{\partial \vec{p}} \bigg|_{t=t_1} \right] \cdot \delta \vec{p}_1 \;=\; 0. \tag{3.31}$$

Eq.(3.31) can add into Eq.(3.30) without loss of generality by multiplying with the real-valued constant variable γ, and then adding into Eq.(3.30). Therefore, the optimal trajectory $(t, \vec{p}^{\,*}, \vec{v}^{\,*})$ must satisfy:

$$\left[\mathcal{H}^{*}\Big|_{t=t_1} \right] \delta t_1 + \left[\gamma \frac{\partial f^{*}}{\partial \vec{p}} \bigg|_{t=t_1} - \vec{\lambda}(t_1) \right] \cdot \delta \vec{p}_1 \;\geq\; 0, \tag{3.32}$$

where $\gamma \in \mathcal{R}$ and can be arbitrary real value. However, the endpoints are not constrained by only Eq.(3.6) but Eq.(3.5) as well. If the endpoint of the optimal state $\vec{p}^{\,*}$ makes w_j inactive, so $w_j(\vec{p}^{\,*}(t_1),t_1) < 0$, and again, $w_j(\vec{p}(t_1+\delta t_1),t_1+\delta t_1) \leq 0$ must hold for the endpoint of the neighborhood $\vec{p}$, which results in:

$$w_j(\vec{p}(t_1+\delta t_1),t_1+\delta t_1) \quad \{>,=, \text{ or } <\} \quad w_j(\vec{p}^{\,*}(t_1),t_1).$$

The above equation places no restriction on $\delta\vec{p}_1$. On the one hand, if it makes w_j active, so $w_j(\vec{p}^{\,*}(t_1),t_1) = 0$, and

$$w_j(\vec{p}(t_1+\delta t_1),t_1+\delta t_1) \quad \leq \quad w_j(\vec{p}^{\,*}(t_1),t_1).$$

The above equation places the restriction on both $\delta\vec{p}_1$ and δt_1, as shown below:

$$\left[\left.\frac{\partial w_j^*}{\partial t}\right|_{t=t_1}\right]\delta t_1 + \left[\left.\frac{\partial w_j^*}{\partial \vec{p}}\right|_{t=t_1}\right]\cdot\delta\vec{p}_1 \quad \leq \quad 0. \tag{3.33}$$

In case the endpoint of the optimal state $\vec{p}^{\,*}(t)$ makes *all* constraints w_j inactive, $\delta\vec{p}_1$ and also δt_1 can be arbitrary values, and in order to satisfy Eq.(3.32), the terms in the parentheses must be zero:

$$\left.\mathcal{H}^*\right|_{t=t_1} = 0 \qquad \text{and} \qquad \gamma\left.\frac{\partial f^*}{\partial \vec{p}}\right|_{t=t_1} - \vec{\lambda}(t_1) = 0. \tag{3.34}$$

Eq.(3.34) expresses the characteristics of the optimal state $\vec{p}^{\,*}(t)$ and optimal control $\vec{v}^{\,*}(t)$ at the time t_1 when all inequality constraints are inactive.

In case the endpoint of the optimal state $\vec{p}^{\,*}(t)$ makes *some/all* constraints w_j active. All active w_j must place the restriction on both $\delta\vec{p}_1$ and δt_1, as shown in Eq.(3.33). So

$$\left[\left.\frac{\partial w_j^*}{\partial t}\right|_{t=t_1}\right]\delta t_1 + \left[\left.\frac{\partial w_j^*}{\partial \vec{p}}\right|_{t=t_1}\right]\cdot\delta\vec{p}_1 \;\leq\; 0, \qquad j\in\mathcal{A}_{t_1}. \tag{3.35}$$

To satisfy Eq.(3.32) when $\delta\vec{p}_1$ and δt_1 are constrained by Eq.(3.35), the Farkas's lemma is employed again, which results in:

$$\begin{aligned} \left.\mathcal{H}^*\right|_{t=t_1} + \sum_{j\in\mathcal{A}_{t_1}}\beta_j\left.\frac{\partial w_j^*}{\partial t}\right|_{t=t_1} &= 0, \\ \left[\gamma\left.\frac{\partial f^*}{\partial \vec{p}}\right|_{t=t_1}\right] - \vec{\lambda}(t_1) + \sum_{j\in\mathcal{A}_{t_1}}\beta_j\left.\frac{\partial w_j^*}{\partial \vec{p}}\right|_{t=t_1} &= 0, \end{aligned} \tag{3.36}$$

where $\beta_j \geq 0$ for all $j\in\mathcal{A}_{t_1}$. Eq.(3.36) expresses the characteristics of the optimal state $\vec{p}^{\,*}(t)$ and optimal control $\vec{v}^{\,*}(t)$ at the time t_1 when some/all inequality constraints are active.

Notice from Eq.(3.34) and Eq.(3.36) that if an inequality constraint becomes active at time t_1 by the optimal state $\vec{p}^{\,*}$, the term $\beta_j\partial w_j^* / \partial t$ and $\beta_j\partial w_j^* / \partial\vec{p}$ will be added. We generalize this by raising the additional equation shown below:

$$\beta_j w_j(\vec{p}^{\,*}(t_1),t_1) \;=\; 0, \qquad j=1,\ldots,N.$$

In summary, the optimal trajectory $(t,\vec{p}^{\,*}(t),\vec{v}^{\,*}(t))$ at time t_1 must satisfy:

$$
\begin{aligned}
\mathcal{H}^*\Big|_{t=t_1} + \sum_{j=1}^{N} \beta_j \frac{\partial w_j^*}{\partial t}\Bigg|_{t=t_1} &= 0, \\
\left[\gamma \frac{\partial f^*}{\partial \vec{p}}\Bigg|_{t=t_1}\right] - \vec{\lambda}(t_1) + \sum_{j=1}^{N} \beta_j \frac{\partial w_j^*}{\partial \vec{p}}\Bigg|_{t=t_1} &= 0, \\
\beta_j w_j(\vec{p}^*(t_1), t_1) &= 0, \qquad j = 1,\ldots,N \\
\beta_j &\geq 0, \qquad j = 1,\ldots,N \\
\gamma &\in \mathcal{R}.
\end{aligned}
\tag{3.37}
$$

For the initial point of the optimal trajectory $(t, \vec{p}^*(t), \vec{v}^*(t))$, the initial point of the state $\vec{p}(t)$ in our problem is fixed in both space and time, and can be known in advance. So,

$$
\vec{p}^*(t_0) = \vec{p}_0 \tag{3.38}
$$

where $\vec{p}_0$ is already known.

Conclusion: If a trajectory $(t, \vec{p}(t), \vec{v}(t))$ is the optimal trajectory to the problem, it must satisfy the necessary conditions defined in Eq.(3.29) along with the boundary conditions defined in Eq.(3.37) and Eq.(3.38).

จุฬาลงกรณ์มหาวิทยาลัย
CHULALONGKORN UNIVERSITY

3.3.3 Sufficient Conditions for Optimality

So far we know that if a trajectory $(t, \vec{p}(t), \vec{v}(t))$ is the optimal trajectory to the problem, which yields the minimum functional E^*, it must satisfy Eq.(3.29). But we cannot say that any trajectory $(t, \vec{p}(t), \vec{v}(t))$ that satisfies Eq.(3.29) is the *(local) minimum* trajectory, because in the previous derivation the only first-order Taylor series was used, causing $E - E^* = 0$ when Eq.(3.29) holds. So, we cannot conclude that it is the minimum trajectory. This is analogous to the problem of finding a point

x that minimizes the function $f(x)$, which we cannot know that the point x that satisfy $f'(x)=0$ is the minimum point unless $f''(x)\geq 0$ is satisfied. Therefore, the sufficient conditions for optimality are essential, and we will examine in this section.

What we need is the conditions that assert $E-E^{*}\geq 0$ about the (local) minimum trajectory $(t,\vec{p}^{*}(t),\vec{v}^{*}(t))$. Remember that the point $(t,\vec{p}^{*}(t),\vec{v}^{*}(t))$ satisfies the necessary conditions defined by Eq.(3.29) and the boundary conditions defined by Eq.(3.37) and Eq.(3.38). From the definition E in Eq.(3.3),

$$\Delta \triangleq E-E^{*}=\int_{t_0}^{t_1}(g-g^{*})\,dt+\int_{t_1}^{t_1+\delta t_1} g\,dt. \tag{3.39}$$

According to the Hamiltonian $\mathcal{H}=g+\vec{\lambda}\cdot\vec{h}$, Eq.(3.39) becomes:

$$\Delta=\int_{t_0}^{t_1}(\mathcal{H}-\mathcal{H}^{*})\,dt+\int_{t_0}^{t_1}\vec{\lambda}\cdot(\vec{h}^{*}-\vec{h})\,dt+\int_{t_1}^{t_1+\delta t_1} g\,dt, \tag{3.40}$$

and we can deduce that $\Delta\geq 0$ from these following steps:

$$\Delta=\int_{t_0}^{t_1}(\mathcal{H}-\mathcal{H}^{*})\,dt+\int_{t_0}^{t_1}\vec{\lambda}\cdot(\vec{h}^{*}-\vec{h})\,dt+\int_{t_1}^{t_1+\delta t_1} g\,dt$$

$$\Delta\overset{(1)}{\geq}\int_{t_0}^{t_1}\left[\frac{\partial\mathcal{H}^{*}}{\partial\vec{p}}\cdot\Delta\vec{p}+\frac{\partial\mathcal{H}^{*}}{\partial\vec{v}}\cdot\Delta\vec{v}\right]dt$$

$$+\int_{t_0}^{t_1}\vec{\lambda}\cdot(\vec{h}^{*}-\vec{h})\,dt+\int_{t_1}^{t_1+\delta t_1} g\,dt$$

$$\Delta \overset{(2)}{=} \int_{t_0}^{t_1} \left[-\dot{\vec{\lambda}} \cdot \Delta\vec{p} - \sum_{j=1}^{N} \left[\alpha_j \frac{\partial w_j^*}{\partial \vec{p}} \cdot \Delta\vec{p} \right] + \frac{\partial \mathcal{L}^*}{\partial \vec{v}} \cdot \Delta\vec{v} \right] dt$$

$$+ \int_{t_0}^{t_1} \vec{\lambda} \cdot (\vec{h}^* - \vec{h})\, dt + \int_{t_1}^{t_1+\delta t_1} g\, dt$$

$$\Delta \overset{(3)}{=} \int_{t_0}^{t_1} \left[-\dot{\vec{\lambda}} \cdot \Delta\vec{p} - \vec{\lambda} \cdot \Delta\dot{\vec{p}} \right] dt$$

$$+ \int_{t_0}^{t_1} \left[-\sum_{j=1}^{N} \alpha_j \frac{\partial w_j^*}{\partial \vec{p}} \cdot \Delta\vec{p} \right] dt + \int_{t_1}^{t_1+\delta t_1} g\, dt$$

$$\Delta \overset{(4)}{=} \int_{t_0}^{t_1} \left[-\frac{d}{dt}(\vec{\lambda} \cdot \Delta\vec{p}) \right] dt$$

$$+ \int_{t_0}^{t_1} \left[-\sum_{j=1}^{N} \alpha_j \frac{\partial w_j^*}{\partial \vec{p}} \cdot \Delta\vec{p} \right] dt + \int_{t_1}^{t_1+\delta t_1} g\, dt$$

$$\Delta \overset{(5)}{\geq} \int_{t_0}^{t_1} \left[-\frac{d}{dt}(\vec{\lambda} \cdot \Delta\vec{p}) \right] dt + \int_{t_1}^{t_1+\delta t_1} g\, dt$$

$$\Delta \overset{(6)}{\approx} -\vec{\lambda}(t_1) \cdot \Delta\vec{p}(t_1) + \vec{\lambda}(t_0) \cdot \Delta\vec{p}(t_0) + g^* \Big|_{t=t_1} \delta t_1$$

$$\Delta \overset{(7)}{=} -\vec{\lambda}(t_1) \cdot \Delta\vec{p}(t_1) + g^* \Big|_{t=t_1} \delta t_1$$

$$\Delta \overset{(8)}{=} -\gamma \left[\frac{\partial f^*}{\partial \vec{p}} \Big|_{t=t_1} \right] \cdot \Delta\vec{p}(t_1) - \sum_{j=1}^{N} \beta_j \left[\frac{\partial w_j^*}{\partial \vec{p}} \Big|_{t=t_1} \right] \cdot \Delta\vec{p}(t_1) + g^* \Big|_{t=t_1} \delta t_1$$

จุฬาลงกรณ์มหาวิทยาลัย
CHULALONGKORN UNIVERSITY

$$\Delta \overset{(9)}{=} -\gamma\left[\left.\frac{\partial f^*}{\partial \vec{p}}\right|_{t=t_1}\right]\cdot\Delta\vec{p}(t_1) - \sum_{j=1}^{N}\beta_j\left[\left.\frac{\partial w_j^*}{\partial \vec{p}}\right|_{t=t_1}\right]\cdot\Delta\vec{p}(t_1)$$

$$+\gamma\left[\left.\frac{\partial f^*}{\partial \vec{p}}\right|_{t=t_1}\right]\cdot\Delta\vec{p}(t_1) + \sum_{j=1}^{N}\beta_j\left[\left.\frac{\partial w_j^*}{\partial \vec{p}}\right|_{t=t_1}\right]\cdot\Delta\vec{p}(t_1)$$

$$-\gamma\left[\left.\frac{\partial f^*}{\partial \vec{p}}\right|_{t=t_1}\right]\cdot\delta\vec{p}_1 - \sum_{j=1}^{N}\beta_j\left[\left.\frac{\partial w_j^*}{\partial \vec{p}}\right|_{t=t_1}\right]\cdot\delta\vec{p}_1$$

$$+\left.\mathcal{H}^*\right|_{t=t_1}\delta t_1$$

$$\Delta \overset{(10)}{=} -\gamma\left[\left.\frac{\partial f^*}{\partial \vec{p}}\right|_{t=t_1}\right]\cdot\delta\vec{p}_1 - \sum_{j=1}^{N}\beta_j\left[\left.\frac{\partial w_j^*}{\partial \vec{p}}\right|_{t=t_1}\right]\cdot\delta\vec{p}_1$$

$$+\left.\mathcal{H}^*\right|_{t=t_1}\delta t_1$$

$$\Delta \overset{(11)}{=} -\gamma\left[\left.\frac{\partial f^*}{\partial \vec{p}}\right|_{t=t_1}\right]\cdot\delta\vec{p}_1 - \sum_{j=1}^{N}\beta_j\left[\left.\frac{\partial w_j^*}{\partial \vec{p}}\right|_{t=t_1}\right]\cdot\delta\vec{p}_1$$

$$-\sum_{j=1}^{N}\beta_j\left.\frac{\partial w_j^*}{\partial t}\right|_{t=t_1}\delta t_1$$

$$\Delta \overset{(12)}{\geq} 0.$$

Explanation:

(1): Assume that $\mathcal{H}$ is convex in ($\vec{p},\vec{v}$).

So $\mathcal{H}-\mathcal{H}^* \geq \left[\partial\mathcal{H}^* / \partial\vec{p}\right]\cdot\Delta\vec{p} + \left[\partial\mathcal{H}^* / \partial\vec{v}\right]\cdot\Delta\vec{v}$.

(2): Use the fact that $\mathcal{H} = \mathcal{L} - \sum \alpha_j w_j$ and $\partial\mathcal{L}^* / \partial\vec{p} = -\dot{\vec{\lambda}}$.

(3): $\partial\mathcal{L}^* / \partial\vec{v} = 0$ and $\Delta\dot{\vec{p}} = \vec{h} - \vec{h}^*$.

(4): $d(\vec{\lambda}\cdot\Delta\vec{p}) = \dot{\vec{\lambda}}\cdot\Delta\vec{p} + \vec{\lambda}\cdot\Delta\dot{\vec{p}}$.

(5): Assume that $\alpha_j(\partial w_j^* / \partial\vec{p})\cdot\Delta\vec{p} \leq 0$ for all $j = 1,\ldots,N$.

(6): The first two terms come from the rule of integration, and the last one from Eq.(3.13).

(7): Since the initial point in our case is fixed, so $\Delta\vec{p}(t_0) = 0$.

(8): Replace $\vec{\lambda}(t_1)$ with the boundary condition in Eq.(3.37).

(9): Replace $g^*\big|_{t=t_1}$ with $\mathcal{H}^*\big|_{t=t_1} - \vec{\lambda}(t_1)\cdot\vec{h}^*\big|_{t=t_1}$, and follow from the fact in Eq.(3.4), Eq.(3.18), and Eq.(3.37).

(10): First four terms are cancelled out.

(11): Replace $\mathcal{H}^*\big|_{t=t_1}$ with the boundary condition in Eq.(3.37).

(12): Assume that $\gamma(\partial f^* / \partial\vec{p})|_{t=t_1}\cdot\delta\vec{p}_1 \leq 0$, and $\beta_j(\partial w_j^* / \partial\vec{p})|_{t=t_1}\cdot\delta\vec{p}_1 + \beta_j(\partial w_j^* / \partial t)|_{t=t_1}\ \delta t_1 \leq 0$.

Conclusion: A trajectory $(t,\vec{p},\vec{v})$ that yields the (local) minimum functional E^*; in other word $E - E^* \geq 0$, must satisfy not only the necessary conditions defined by Eq.(3.29) and the boundary conditions in Eq.(3.37), but these following conditions as well:

$$\mathcal{H} \text{ is convex in } (\vec{p},\vec{v}) \tag{3.41}$$

$$\alpha_j\left[\frac{\partial w_j^*}{\partial\vec{p}}\right]\cdot\Delta\vec{p} \ \leq\ 0, \qquad j = 1,\ldots,N. \tag{3.42}$$

$$\gamma\frac{\partial f^*}{\partial\vec{p}}\bigg|_{t=t_1}\cdot\delta\vec{p}_1 \ \leq\ 0. \tag{3.43}$$

$$\beta_j \left[\left[\frac{\partial w_j^*}{\partial \vec{p}} \bigg|_{t=t_1} \right] \cdot \delta \vec{p}_1 + \left[\frac{\partial w_j^*}{\partial t} \bigg|_{t=t_1} \right] \delta t_1 \right] \leq 0, \qquad j = 1, \ldots, N. \tag{3.44}$$

3.4 Dynamic Programming

Dynamic programming is a useful technique in the diverse areas especially in computer science for solving complex problems by breaking the problem down into simpler subproblems. The important thing is that the problems must have the properties of the optimal substructure and overlapping subproblems. A problem is said to have optimal substructure if the optimal solution of the given problem contains within the optimal solutions of its subproblems. A problem is said to have overlapping subproblems if the problem can be broken down into the subproblems, and once the solutions of the subproblems are obtained, they can be reused several times until the solution of the problem comes out. Dynamic programming takes the advantage of not always generating the new subproblems to speed up the performance, and it is better in term of computation time to find out the optimal solution than naive recursive approaches like depth-first search and breadth-first search.

จุฬาลงกรณ์มหาวิทยาลัย
CHULALONGKORN UNIVERSITY

CHAPTER 4

METABOLIC-ENERGY-MINIMAL SHORT-TERM PATH PLANNING

4.1 Overview of Our Crowd Simulation System

Our crowd simulation system assumes that each pedestrian in bidirectional flow is already given the desired walking direction to one of the exits of a passageway, which can be simply defined by any GPP; for example, in a graph-based approach, the desired walking direction may be the tangent to a piecewise smooth curve at a point a pedestrian is corresponding to. Given the desired walking direction, the pedestrian then employs the MEM by firstly perceiving nearby people, secondly predicting their walking paths, and lastly planning for the energy-minimal path that compromises between the walking energy expended and the distance to destination. The energy-minimal path describes not only the spatial information but also the temporal one, which serves as the desired velocity at the present time for the considered pedestrian. Finally, the LCA will exploit the desired velocity as an input to compute the actual one in the sense that the pedestrian attempts to walk along the energy-minimal path simultaneously with preventing collisions with the nearby walkers.

จุฬาลงกรณ์มหาวิทยาลัย

Algorithm 1 Crowd Simulation in Bidirectional Flow

```
while simulating do
    for each pedestrian i do
        d_i ← ComputeDesiredWalkingDirGPP()
        v_i,des ← EnergyMinimalPathMEM(d_i)
        v_i,act ← LocalCollisionAvoidance(v_i,des)
        UpdatePosition(v_i,act)
    end for
end while
```

Algorithm 1. shows our simulation loop where the desired walking direction, the desired velocity, and the actual velocity of the *i*th pedestrian are represented by $\vec{d}_i$, $\vec{v}_{i,\text{des}}$, and $\vec{v}_{i,\text{act}}$ respectively. The function *ComputeDesiredWalkingDirGPP*(•) will be called in every time step to allow the pedestrian to anytime change his mind

on the direction towards an exit of a passageway, but in case the direction is fixed, calling it once is enough. Our main contribution is in finding the energy-minimal path in the MEM, which performs through the function *EnergyMinimalPathMEM*(•) and will be detailed in the next section. The proposed MEM can be seamlessly connected with any previous LCA methods by using the desired velocity as a connector.

4.2 Metabolic-Energy-Minimal Short-Term Path Planning (MEM)

Our MEM computes the desired velocity $\vec{v}_{i,\text{des}}$ for each pedestrian based on the principle of least effort and the biomechanical walking energy. The problem we are dealing with was shown in Figure 2. Instead of planning a route to the one end of the corridor, the considered pedestrian i, which is depicted by the red circle in Figure 2, will plan its walking path toward the front line being far away from his current position with a distance specified by the user. We assume that the pedestrian i is positioned at the origin of the reference frame x - y and only responses to the perceived people in front.

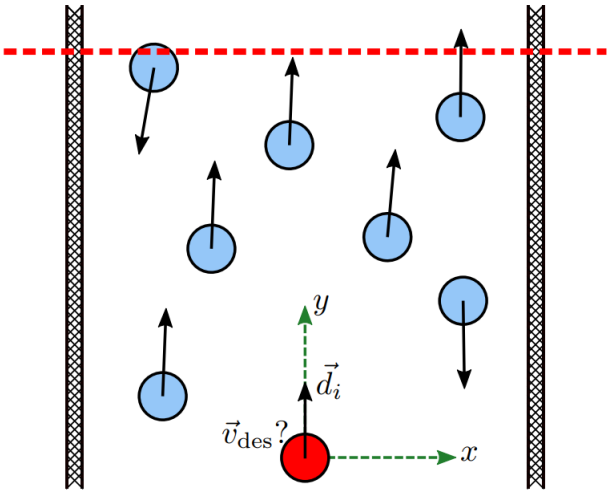

Figure 2. The red pedestrian, who is located at the origin of the reference frame, is desired to walk toward the front line, or the red dashed line, with the lowest walking energy expenditure

The future position of the perceived people in front will be predicted by two nuanced ways, subject to the distance to the pedestrian i. If the distance is below some threshold l_{th}, the future position is obtained by linearly extrapolating its current velocity, otherwise the projected current velocity onto the desired walking direction $\vec{d}_i$ of the pedestrian i. The threshold l_{th} is set to 3.66 meters. This is the maximum distance of the social space [59] where the direct interactions and responses between the real humans happen. For the people in front beyond the social space (farther than the threshold l_{th}), prediction by using the projected velocity onto the desired walking direction $\vec{d}_i$ is reasonable enough in case of bidirectional crowd flow where two pedestrians have a high tendency to meet each other at a future time, if extrapolating the current velocity is used instead, the future position at a large time period may lie outside the corridor and cause no influence on the pedestrian i.

The measurement for the walking energy is solely based on the biomechanical study of the real human walking [55] in which the oxygen uptake of a subject walking on a treadmill at varying speeds was recorded, resulting in a mathematical equation that manifests the relationship between the instantaneous metabolic energy expenditure and the walking speed, as shown below.

จุฬาลงกรณ์มหาวิทยาลัย
CHULALONGKORN UNIVERSITY

$$\frac{dE}{dt} = m\left[e_s + e_w \left\|\vec{v}(t)\right\|^2\right] \tag{4.1}$$

where E is the total metabolic energy measured in joules (J), m is the mass measured in kilograms (kg), $\vec{v}(t)$ is the velocity at time t measured in m/s, e_s and e_w are the constants measured in J/kg/s and Js/kg/m^2 respectively, and $\|\cdot\|$ is the Euclidean norm. The constant e_s and e_w can be viewed as the rates of the energy expended while standing and walking, respectively. These constants are unique for each pedestrian, and for the average human, the constant e_s is equal to 2.23 J/kg/s while the constant e_w is 1.25 Js/kg/m^2.

According to Eq. (4.1), we can compute the total metabolic energy expended by the pedestrian i over arbitrary time period Δt by using the following equation.

$$E = m \int^{\Delta t} \left[e_s + e_w \left\| \vec{v}(t) \right\|^2 \right] dt \tag{4.2}$$

The pedestrian i will plan its walking path from the current time t_c to the unknown future time t_e (time at which the pedestrian i reaches the front line), so $\Delta t = t_e - t_c$.

4.3 Constrained Optimization Problem

From the principle of least effort [54], the pedestrian i is supposed to walk with the least amount of energy expenditure. So we compute the desired velocity $\vec{v}_{i,\text{des}}(t)$ for the pedestrian i over time period $[t_c, t_e]$ such that the total metabolic energy E is minimized:

$$\vec{v}_{i,\text{des}}(t) = \underset{\vec{v}_i(t) \in \mathcal{V}}{\operatorname{argmin}}\ E \tag{4.3}$$

where $\mathcal{V}$ is a set of collision-free velocities over time period $[t_c, t_e]$. Although our objective function is similar to PLEdestrians [43], they are different in purposes. In PLEdestrians, a desired velocity is given, and the energy-minimal actual velocity is then computed. Refer to Algorithm 1, PLEdestrians addresses the problem in *LocalCollisionAvoidance*(·) function.

To define a set of collision-free velocities $\mathcal{V}$, the mathematical representation of the front line and the perceived people in front must be well established. We ignore the boundary of the corridor momentarily to examine the energy-minimal walking characteristics of the pedestrian i against the perceived

people. The front line and the jth perceived people at time t are illustrated by the implicit equations $f(\vec{p})=0$ and $w_j(\vec{p},t)=0$, respectively, where $\vec{p}$ is a point (x,y) in the reference frame. The geometric shape of jth perceived people is defined as a circle with the radius (r_i+r_j), where r_i and r_j are the radius of the considered pedestrian i and jth perceived people. So,

$$w_j(\vec{p},t) \triangleq (r_j+r_i)^2 - \left\|\vec{p}-\vec{p}_j(t)\right\|^2 \tag{4.4}$$

where $\vec{p}_j(t)$ is the position of the jth perceived people at time t. For the future position of the jth perceived people, we linearly extrapolate its current velocity when the distance to considered pedestrian i below the threshold l_{th}, otherwise the projected one onto $\vec{d}_i$, so

$$\vec{p}_j(t)=\begin{cases} \vec{p}_j(t_c)+(t-t_c)\vec{v}_j(t_c), & \left\|\vec{p}_j(t_c)\right\| \leqslant l_{\text{th}} \\ \vec{p}_j(t_c)+(t-t_c)(\vec{v}_j(t_c)\cdot\vec{d}_i)\vec{d}_i, & \text{otherwise.} \end{cases} \tag{4.5}$$

With above definition, a velocity $\vec{v}_i(t)$ in a set $\mathcal{V}$ must conform to:

$$\begin{aligned} \dot{\vec{p}}_i(t) &= \vec{v}_i(t) \\ w_j(\vec{p}_i(t),t) &\leq 0, \qquad j=1,\ldots,N \\ f(\vec{p}_i(t_e)) &= 0 \end{aligned} \tag{4.6}$$

where $\vec{p}_i(t)$ is the position of the pedestrian i at time t, and N is the number of perceived people. The first equation describes the motion of the pedestrian i, the second forces the pedestrian i not to collide with the perceived people, and the last one ensures that the pedestrian i must reach the front line at time $t=t_e$.

4.4 Metabolic-Energy-Minimal Walking Characteristics

The objective function in Eq.(4.3) and the constraints in Eq.(4.6) are investigated to compute the energy-minimal walking velocity which mathematically expressed by $\vec{v}_{i,\text{des}}(t)$ for $t \in [t_c, t_e]$.

4.4.1 Result from Constrained Optimization Problem

First of all, we change the objective function in Eq.(3.3) by using these following functions: (1) $g(t,\vec{p}(t),\vec{v}(t)) = m(e_s + e_w \|\vec{v}(t)\|^2)$, (2) $t_0 = t_c$ and $t_1 = t_e$, and (3) $\vec{h}(t,\vec{p}(t),\vec{v}(t)) = \vec{v}(t)$, then eliminating the variable $\vec{\lambda}$ in Eq.(3.29), which results in the optimal acceleration:

$$\vec{a}_i^{\,*}(t) = -\frac{1}{me_w}\sum_{j=1}^{N}\alpha_j(t)\,(\vec{p}_i^{\,*}(t) - \vec{p}_j(t)) \tag{4.7}$$

$$\alpha_j(t) w_j(\vec{p}_i^{\,*}(t),t) = 0 \quad \text{and} \quad \alpha_j(\mathrm{t}) \geq 0 \tag{4.8}$$

And by using Eq.(3.37), the characteristics of the optimal velocity at time t_e is obtained as follows:

$$\vec{v}_i^{\,*}(t_e) = -\frac{1}{2me_w}\left[\gamma\frac{\partial f}{\partial \vec{p}} + \sum_{j=1}^{N}\beta_j\frac{\partial w_j}{\partial \vec{p}}\right]\Bigg|_{\vec{p}_i^{\,*},t_e} \quad \text{and} \quad \gamma \in \mathcal{R} \tag{4.9}$$

$$\left\|\vec{v}_i^{\,*}(t_e)\right\| = \sqrt{\frac{e_s}{e_w} + \frac{1}{me_w}\sum_{j=1}^{N}\beta_j\frac{\partial w_j}{\partial t}\Bigg|_{\vec{p}_i^{\,*},t_e}} \tag{4.10}$$

$$\beta_j w_j(\vec{p}_i^{\,*}(t_e),t_e) = 0 \quad \text{and} \quad \beta_j \geq 0 \tag{4.11}$$

Considering the Hamiltonian $\mathcal{H} = g + \vec{\lambda} \cdot \vec{h}$, we get:

$$\mathcal{H} = m\left[e_s + e_w \left\|\vec{v}(t)\right\|^2\right] + \vec{\lambda} \cdot \vec{v}(t),$$

where the Hessian matrix of this $\mathcal{H}$, corresponding to $\vec{p}$ and $\vec{v}$ where $\vec{p}, \vec{v} \in \mathcal{R}^2$, is:

$$\text{Hessian}(\mathcal{H}) = \begin{bmatrix} 0 & 0 & 0 & 0 \\ 0 & 0 & 0 & 0 \\ 0 & 0 & 2me_w & 0 \\ 0 & 0 & 0 & 2me_w \end{bmatrix}$$

which is positive-definite matrix. This means that the Hamiltonian $\mathcal{H}$ is convex in $(\vec{p}, \vec{v})$. So the sufficient condition in Eq.(3.41) is satisfied.

For the inequality constraints $w_j(\vec{p}(t), t) \leq 0$, we use the circle equation to represent a virtual pedestrian's boundary. Mathematically,

$$w_j(\vec{p}, t) \triangleq r^2 - \left\|\vec{p} - \vec{p}_j(t)\right\|^2,$$

and in addition, we obtain the fact that

$$w_j(\vec{p}(t), t) - w_j(\vec{p}^*(t), t) = \frac{\partial w_j^*}{\partial \vec{p}} \cdot \Delta\vec{p}(t) - \left\|\Delta\vec{p}(t)\right\|^2.$$

At a certain time t, if the optimal point $\vec{p}^*(t)$ makes the constraint w_j inactive $(w_j < 0)$, so $\alpha_j = 0$, causing the sufficient condition in Eq.(3.42) to be satisfied. If the optimal point $\vec{p}^*(t)$ makes w_j active $(w_j = 0)$ as shown in Figure 3, every neighborhood $\vec{p}(t)$ that lies in the left half plane specified by the tangent line at the

optimal point $\vec{p}^{*}(t)$ will always cause $\partial w_j^{*} / \partial \vec{p} \cdot \Delta \vec{p} \leq 0$, and due to $\alpha_j \geq 0$, the sufficient condition in Eq.(3.42) is then satisfied. However, for the neighborhoods $\vec{p}(t)$ that lie in the right half plane and yield $w_j < 0$, they could produce $\partial w_j^{*} / \partial \vec{p} \cdot \Delta \vec{p} \geq 0$. As $\Delta \vec{p}(t)$ is infinitesimal, the admissible neighborhood $\vec{p}(t)$ within some small radius ϵ will cause $\partial w_j^{*} / \partial \vec{p} \cdot \Delta \vec{p} \longrightarrow 0$, as shown in the bottom-right rectangle in Figure 3. Therefore, the sufficient condition in Eq.(3.42) is satisfied.

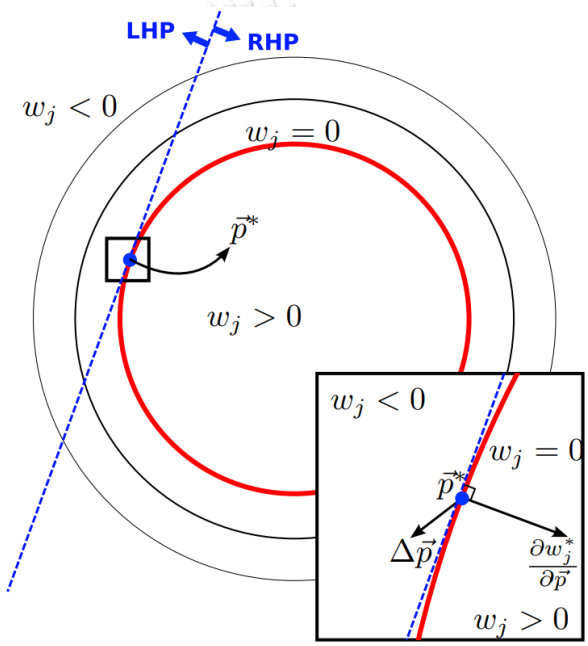

CHULALONGKORN UNIVERSITY

Figure 3. Graphical meaning of the inequality constraint $w_j(\vec{p}(t),t) \leq 0$ used in our optimization problem. Suppose at a certain time t the optimal point $\vec{p}^{*}(t)$ on the optimal trajectory makes the constraint w_j active as shown in the figure, we can conclude that $\partial w_j^{*} / \partial \vec{p} \cdot \Delta \vec{p} \leq 0$ holds for every neighborhood $\vec{p}(t)$, when the distance between those two points ($\Delta \vec{p}$) is infinitesimal.

For the endpoint constraint $f(\vec{p}(t)) = 0$, the endpoint of the optimal trajectory $(\vec{p}^{*}(t_1))$ and the endpoint of the neighboring trajectory $(\vec{p}(t_1 + \delta t_1))$ must lie on

this curve f, and because of the infinitesimal distance between these two endpoints, we obtain:

$$\left[\left.\frac{\partial f^*}{\partial \vec{p}}\right|_{t=t_1}\right]\cdot \delta\vec{p}_1 = 0.$$

This results in the satisfaction to the sufficient condition in Eq.(3.43) no matter what γ is. For the graphical description, please see Figure 4.

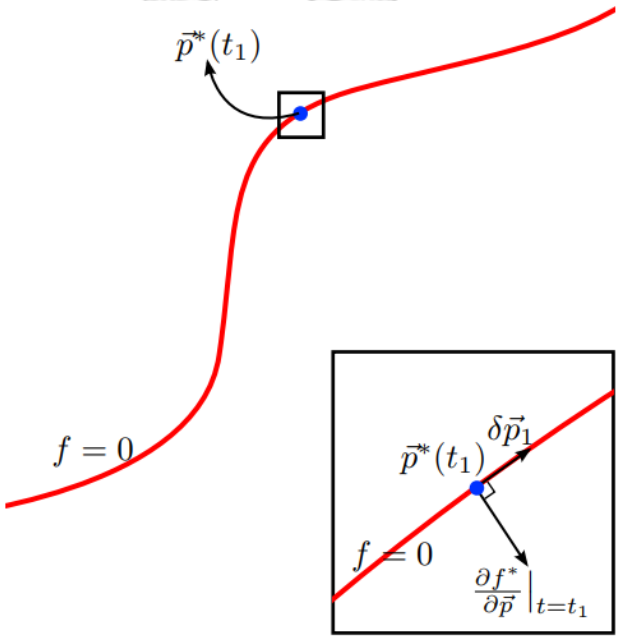

Figure 4. Graphical meaning of the endpoint constraint $f(\vec{p}(t_1)) = 0$. *Since the endpoints of the optimal trajectory and the neighborhood must lie on this curve, so we can conclude that* $(\partial f^* / \partial \vec{p})|_{t=t_1} \cdot \delta\vec{p}_1 = 0$ *holds for every neighborhood of the optimal point* $\vec{p}^*(t_1)$, *when* $\delta\vec{p}_1$ *is infinitesimal.*

The explanation for the satisfaction towards the sufficient condition in Eq.(3.44) is similar to one in Eq.(3.42) except that instead of examining the level curves $w_j(\vec{p},t)$ at a specific time t as shown in Figure 3, the level surfaces emerge

when the time t is considered. Because a virtual pedestrian is supposed to walk with constant velocity in MEM and its shape is simplified by using circle, so its level surface can be demonstrated by extruding a circle in an upward direction (in time direction), resulting in a slanted cylinder if a pedestrian walks with some speed; otherwise a straight cylinder. In case the optimal point $\vec{p}^{*}(t_1)$ makes the constraint w_j inactive $(w_j < 0)$, so $\beta_j = 0$, causing the sufficient condition in Eq.(3.44) to be satisfied. Likewise, if the optimal point $\vec{p}^{*}(t_1)$ makes w_j active $(w_j = 0)$, every neighborhood $\vec{p}(t_1 + \delta t_1)$ in an outer region specified by the tangent plane at the optimal point $\vec{p}^{*}(t_1)$ (similar to the left half plane in Figure 3) always satisfy Eq.(3.44). However, for the neighborhoods $\vec{p}(t_1 + \delta t_1)$ that lie in the inner region (similar to the right half plane in Figure 3) and yield $w_j < 0$, they could cause the left-hand side of Eq.(3.44) to greater than or equal to zero. But $\delta\vec{p}_1$ is infinitesimal, those terms will approach to zero. Therefore, the sufficient condition in Eq.(3.44) is satisfied.

As all sufficient conditions are attained, any position $\vec{p}(t)$ and the velocity $\vec{v}(t)$ that conform to the energy-minimal walking characteristics, defined by Eq.(4.7) – (4.11), are the solution that yields the (local) minimum walking energy.

จุฬาลงกรณ์มหาวิทยาลัย
CHULALONGKORN UNIVERSITY

4.4.2 Useful Walking Characteristics

In summary, the result of the investigation provides us the following equations:

$$\vec{a}_i^{*}(t) = -\frac{1}{me_w}\sum_{j=1}^{N}\alpha_j(t)\left[\vec{p}_i^{*}(t) - \vec{p}_j(t)\right] \tag{4.12}$$

$$\alpha_j(t)w_j(\vec{p}_i^{*}(t),t) = 0 \quad \text{and} \quad \alpha_j(\mathrm{t}) \geq 0 \tag{4.13}$$

$$\vec{v}_i^{\,*}(t_e) = -\frac{1}{2me_w}\left[\gamma\frac{\partial f}{\partial \vec{p}} + \sum_{j=1}^{N}\beta_j\frac{\partial w_j}{\partial \vec{p}}\right]\Bigg|_{\vec{p}_i^{\,*},t_e} \quad \text{and} \quad \gamma \in \mathcal{R} \tag{4.14}$$

$$\left\|\vec{v}_i^{\,*}(t_e)\right\| = \sqrt{\frac{e_s}{e_w} + \frac{1}{me_w}\sum_{j=1}^{N}\beta_j\frac{\partial w_j}{\partial t}\Bigg|_{\vec{p}_i^{\,*},t_e}} \tag{4.15}$$

$$\beta_j w_j(\vec{p}_i^{\,*}(t_e), t_e) = 0 \quad \text{and} \quad \beta_j \geq 0 \tag{4.16}$$

where $\vec{a}_i(t)$ is the acceleration of the pedestrian i at time t, and the asterisk means the variable is computed at the optimal point. Eq.(4.12) and Eq.(4.13) explain the characteristic of the optimal acceleration that make the pedestrian i expend the (local) minimal metabolic energy. While Eq.(4.14) - Eq.(4.16) tell us about the optimal velocity $\vec{v}_i(t)$ at time $t = t_e$ (time at which the pedestrian i touches the front line f).

The energy-minimal walking characteristics that we can deduce from Eq.(4.12) – (4.16) are:

จุฬาลงกรณ์มหาวิทยาลัย
Chulalongkorn University

Characteristic A.1: For any time period when the pedestrian i walks without touching any perceived people, he must walk with constant velocity.

Characteristic A.2: For any time period when the pedestrian i touches one of the perceived people; in other words, walks on a circle boundary w_j, the relative velocity must be tangent to the circle, and the relative speed must be constant throughout the time when he is touching.

A.1 and A.2 result from observing Eq.(4.12) and Eq.(4.13). Considering the walking characteristics at the time period when pedestrian i does not touch any

perceived people at the optimal position $\vec{p}_i^{\,*}(t)$, we get $w_j(\vec{p}_i^{\,*}(t),t) < 0$ and from Eq.(4.13) we get $\alpha_j(t) = 0$ for all $j = 1,...,N$. This results in zero acceleration $\vec{a}_i^{\,*}(t)$ (constant velocity) in Eq.(4.12) (A.1). Now considering if the pedestrian i touches the jth perceived people (walk on a circle boundary w_j), we get $w_j(\vec{p}_i^{\,*}(t),t) = 0$ and then $\alpha_j(t) \geq 0$. If $\alpha_j(t) = 0$, $\vec{a}_i^{\,*}(t) = 0$ and its velocity is constant. But the pedestrian i is assumed to walk on the circle boundary w_j in this period of time so this case cannot happen, forcing $\alpha_j(t) > 0$. When $\alpha_j(t) > 0$, the direction of $\vec{a}_i^{\,*}(t)$ will point to the center of the circle w_j due to the term $\vec{p}_j(t) - \vec{p}_i^{\,*}(t)$. Note that the velocity of the jth perceived people is constant as explained in Eq.(4.5), so $\vec{a}_i^{\,*}(t)$ can be viewed as a relative acceleration of the pedestrian i against the jth perceived people, and since its direction points to the center, the pedestrian i will undergo the uniform circular motion on this period, and this results to A.2.

Characteristic B.1: At the time t_e (when the pedestrian i reaches the front line f), if he does not simultaneously touch any perceived people, his velocity at that time must be perpendicular to the front line f, and his speed must be equal to $\sqrt{e_s / e_w}$.

Characteristic B.2: At the time t_e (when the pedestrian i reaches the front line f), if he simultaneously touches one of the perceived people, his velocity at that time depends on his state at the time before he reaches the front line f.

B.1 and B.2 are the consequence of observing the boundary conditions at time t_e, as shown in Eq.(4.14) - Eq.(4.16). If the pedestrian i reaches the front line without touching any perceived people at time t_e, we obtain $w_j(\vec{p}_i^{\,*}(t_e),t_e) < 0$ and then $\beta_j = 0$ for all $j = 1,...,N$ in Eq.(4.16). Therefore, the velocity $\vec{v}_i^{\,*}(t_e)$ in Eq.(4.14) must be parallel to the gradient of f (the normal of the front line f) at the position $\vec{p}^{\,*}(t_e)$, and its magnitude must be equal to $\sqrt{e_s / e_w}$ as depicted in Eq.(4.15). This results to B.1. In case he touches one of the perceived people at the

time t_e, so $w_j(\vec{p}_i^{\,*}(t_e),t_e)=0$ and $\beta_j \geq 0$, which gives $\vec{v}_i^{\,*}(t_e)$ the additional dependency on the gradient of w_j (the normal of the circle boundary w_j). As the position $\vec{p}_i^{\,*}(t)$ and the velocity $\vec{v}_i^{\,*}(t)$ are continuous for all time $t \in [t_c, t_e]$, and $\vec{p}_i^{\,*}(t_e)$ lies on the circle boundary w_j, if the position before he reaches the front line f, denoted by $\vec{p}_i^{\,*}(t_e - \epsilon)$ where ϵ is a small positive infinitesimal quantity, does not touch any circle boundary, the velocity $\vec{v}_i^{\,*}(t_e)$ will be characterized by A.1. But if $\vec{p}_i^{\,*}(t_e - \epsilon)$ lies on a circle boundary w_j, A.2 tells us that he is moving in a uniform circular motion at that time and keeps doing this until the time t_e, so the velocity $\vec{v}_i^{\,*}(t_e)$ will be characterized by A.2.

Characteristic C.1: If there is no perceived people, the pedestrian i must walk straight with the constant speed $\sqrt{e_s / e_w}$ in the direction that is perpendicular to the front line f.

Characteristic C.2: If all perceived people stand still, the pedestrian i must walk with constant speed $\sqrt{e_s / e_w}$ throughout the time along the shortest path towards the front line.

จุฬาลงกรณ์มหาวิทยาลัย
CHULALONGKORN UNIVERSITY

C.1 and C.2 explain the walking characteristics in special scenarios. C.1 simply deduces from A.1 and B.1, while C.2 from A.1, A.2, and Eq.(4.15) with the removal of the time derivatives of all w_j. Notice that the walking speed formula $\sqrt{e_s / e_w}$ matches the most efficient walking speed of the average human studied in the biomechanics [55], $\sqrt{2.23 / 1.25} = 1.34$ m/s.

4.5 Near-Global Optimal Solution

A velocity $\vec{v}_i^{\,*}(t)$ that conforms to the above walking characteristics is the local optimal solution to the problem. To find the global one, all possible $\vec{v}_i^{\,*}(t)$

need to be given but calculating each velocity $\vec{v}_i^{\,*}(t)$ analytically is not trivial because the transition at a point between A.1 and A.2 is restricted to be continuous. So, we present the approximation method by replacing a circle w_j with two perpendicular lines, one is parallel to the x-axis of the reference frame, which we called a horizontal line, while the other one is parallel to the y-axis, called a vertical line. The intersection point of these lines is at the center of a circle w_j, and the endpoints of each line are at the middle between the corners of the inner and outer rectangles as shown in Figure 5. When the pedestrian i touches the jth perceived people in a period of time (A.2), he will walk between these endpoints instead of the circle boundary. If the endpoints are at the corners of the inner rectangle in Figure 5(b), the pedestrian i will think that he can walk through two adjacent perceived people, but actually he cannot. If the endpoints are at the corners of the outer rectangle, he will think that he cannot walk through, but actually he can. To compromise these situations, we choose to use the middle points instead.

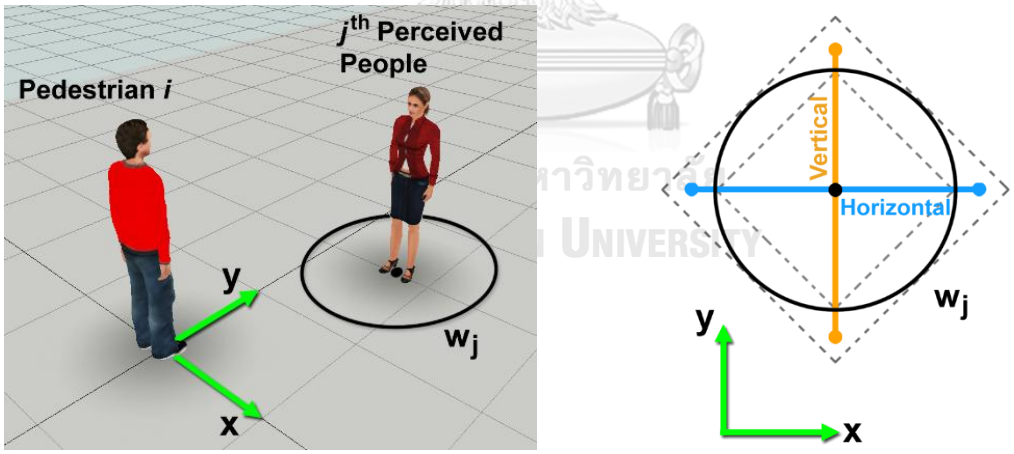

(a) (b)

Figure 5. Representation of perceived people. (a) The jth perceived people is represented by the circle equation w_j. (b) The approximation of w_j.

With this approximation, the energy-minimal paths that conforms to the aforementioned walking characteristics turn out to be piecewise linear curves (a

connected sequence of line segments) in space-time coordinate system of the pedestrian i as shown in Figure 6. We define without loss of generality that the state at time $t = t_c$ happens at $t = 0$ in this space-time coordinate, and the current position of the pedestrian i is $(x, y, t) = \vec{0}$. The horizontal and vertical lines generate two perpendicular planar strips. The front line f creates a plane parallel to the time axis, as shown in Figure 6(b).

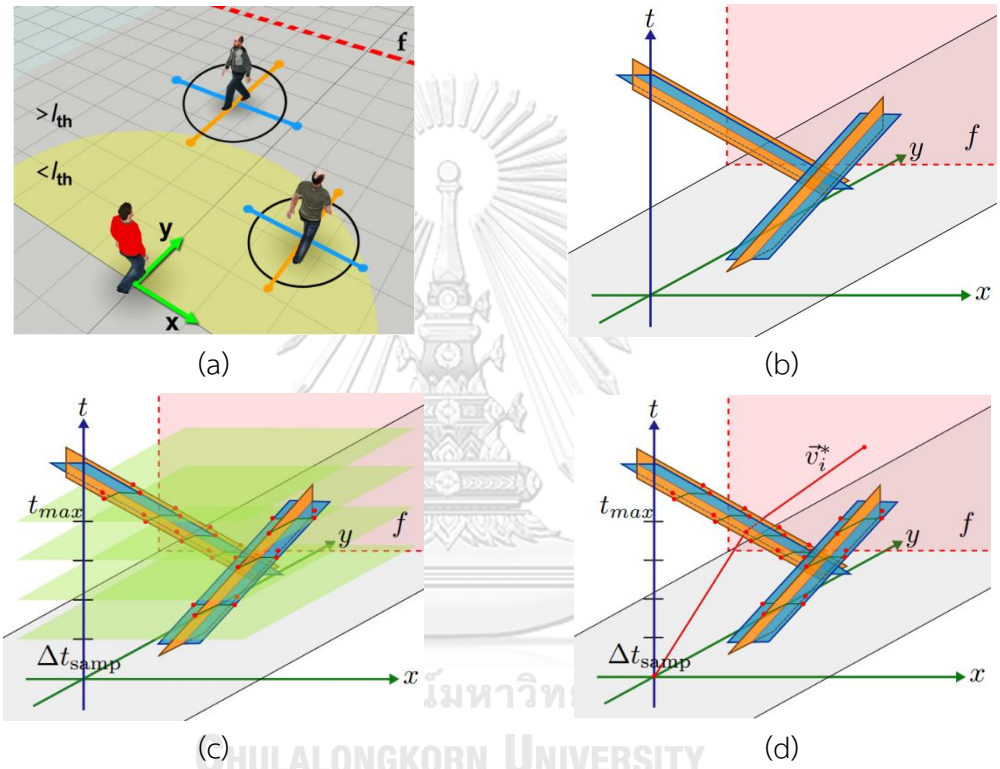

Figure 6. Near-global energy-minimal velocity. (a) Pedestrian i perceived two people in front. The future position of the outside-l_{th}-zone pedestrian is predicted by extrapolating its projected velocity and extrapolating the current velocity for the inside one. (b) Horizontal and vertical lines of each perceived people generate two perpendicular planar strips, and the front line f creates a plane in space-time coordinate system. (c) The sampling time and maximum time are defined to discretize the time axis into levels to construct critical points. (d) The energy-minimal velocity is computed from $\vec{v}_i^*$ obtained by the dynamic programming technique with the knowledge of the energy-minimal walking characteristics.

CHULALONGKORN UNIVERSITY

To find the energy-minimal path, the time axis will be discretized into levels according to the user-defined sampling time Δt_{samp} and the maximum time $t_{\max}$ (Figure 6(c)). At each level, the endpoints of the horizontal and vertical lines are defined as the *critical points*, which perform as the transition points between A.1 and A.2. For the level $t = 0$, there is only one critical point locating at the origin ($\vec{\mathbf{0}}$). Instead of naively searching the energy-minimal path from the critical point at $t = 0$ to the plane f, we use the dynamic programming technique by finding the energy-minimal path starting at the critical points on the top-most level ($t = t_{\max}$), and then the critical points on the lower level, until the critical point $\vec{\mathbf{0}}$ is reached.

For each critical point being examined, two types of line segments must be considered, based on the energy-minimal walking characteristics; (1) a $\sqrt{e_s / e_w}$-slope line segment from the critical point being examined to the closest point on the plane f (B.1), and (2) a line segment from the critical point being examined to the critical points on the higher levels (A.1 and A.2). A line segment will be selected as a candidate for constituting the energy-minimal path if no collision with the perceived people occurs, and thanks to each planar strip, the collision detection is very simple by checking only line-plane intersection. If the latest-examined line segment and its successor promote the lowest energy, such line segment and its successor will be stored at the critical point being examined, and they will be used as a successor for the critical points on the lower level. If the critical point $\vec{\mathbf{0}}$ is examined and there is no connected sequence of line segments from the critical point $\vec{\mathbf{0}}$ to the plane f, the pedestrian i will be given the desired velocity $\sqrt{e_s / e_w}\,\vec{d}_i$, but if there is a sequence (Figure 6(d)), the desired velocity will be computed from the first line segment (line attached to the critical point $\vec{\mathbf{0}}$) by the following equation:

$$\vec{v}_{i,\text{des}}(t_c) = \frac{(\overrightarrow{\mathbf{cp}}_1 - \overrightarrow{\mathbf{cp}}_0)_{xy}}{(\overrightarrow{\mathbf{cp}}_1 - \overrightarrow{\mathbf{cp}}_0)_t} \tag{4.17}$$

where $\overrightarrow{\mathbf{cp}}_1$ and $\overrightarrow{\mathbf{cp}}_0 (= \vec{\mathbf{0}})$ are the critical points that constitute the first line segment.

4.6 Line Segment Pruning

To improve computational performance, line segments that agree with the following conditions will be pruned before checking the line-plane intersection: (1) one of the critical points at the end of a line segment lies inside a circle w_j, (2) the speed computed from the slope of a line segment exceeds the maximum speed of the pedestrian i, (3) a part of a line segment lies outside the corridor, (4) the successor of a line segment does not reach the plane f, (5) a line segment and its successor produce more energy than the previously-examined one, (6) in case the pedestrian i is restricted to plan his walking path only in the forward direction (the positive direction of the y-axis), a line segment that points to the negative direction of the y-axis will be pruned.

Moreover, if we found a $\sqrt{e_s / e_w}$ -slope line segment from a critical point being examined to the closest point on the plane f, we can discard the line segments between levels since the $\sqrt{e_s / e_w}$ -slope line segment produces the most minimal walking energy from the critical point being examined.

4.7 The constant $\mathbf{e_s}$, $\mathbf{e_w}$, and $\mathbf{t_{max}}$

As pedestrians walk at different preferred speed due to their own physiological attributes, for examples, a tall man naturally walks faster than a short one, we handle this diversity in our crowd simulation by setting the constant e_s and e_w for each virtual pedestrian on the assumption that virtual pedestrians expend the same amount of metabolic energy while standing but different while walking. That is:

$$e_s = 2.23$$
$$e_w = \frac{e_s}{v_{\text{pref}}^2} \tag{4.18}$$

where v_{pref} is the preferred speed of a virtual pedestrian. The above assumption comes from the situation when a tall and a short man are at the same position and would like to walk to the same location on the condition that they must reach that location at the same time. The tall man naturally walks faster than the short one by his preferred speed, making the tall man expend the lowest energy, whereas the short one must accelerate himself to pursue the tall man, making the short man walk with higher speed than he prefers, so the short man must spend more energy while walking (e_w) for the instantaneous acceleration, and this conduces to Eq.(4.18).

For the time $t_{\max}$, it should be equal to or greater than the time t_e to secure the energy-minimal walking path towards the front line f, however, the time t_e cannot be known in advance. Nevertheless, $t_{\max}$ must be greater than the time t_e in the situation when the pedestrian i walks without the perceived people in front (C.1), so the lower bound for $t_{\max}$ is $c\sqrt{e_w / e_s}$, where c is the minimum distance to the front line f. For the upper bound, we define it from the situation when the pedestrian i is closely obstructed by all perceived people which horizontally-packed into a single row, so the pedestrian i must walk to the left or right to avoid the perceived people before walking straight to the front line f. Therefore,

$$c\sqrt{\frac{e_w}{e_s}} \leq t_{\max} \leq \left[(\text{largest}_{r_j} + r_i)N + c\right]\sqrt{\frac{e_w}{e_s}} \tag{4.19}$$

where largest_{r_j} is the largest radius among the radii of the perceived people.

CHAPTER 5
RESULTS AND DISCUSSION

In this section, we will show the results through a set of scenarios, and discuss the efficiency by comparing with the previous work and the real-world bidirectional crowd flow. We implemented our work in C++ and used OpenGL for visualization on a 64-bit machine with 8GB of RAM, an Intel i7-2600 3.40GHz processor, and with the NVIDIA Geforce GTX 550 Ti.

5.1 Lane Changing and Overtaking Behavior

The first scenario was shown in Figure 7(a) where the red and yellow pedestrians are walking upward with the desired speed 1.5 m/s and 0.5 m/s respectively, and the three green pedestrians are walking downward with 1.3 m/s. The initial position of the red pedestrian slants a bit to the right side of the yellow one. We compare our method with the social force model, the velocity-based PLEdestrians, and the counterflow model. Since the original social force and the velocity-based models allow the simulated pedestrians to perceive the people in back, causing the people in front to be pushed and/or sidestep, these behaviors should not occur in normal situation of bidirectional crowd flow, so we modified by restricting the visual angle to 180 degrees. For our approach, the front line f is set to be a straight line $y = c$ where c is the planning distance. In this scenario, we set $c = 7\,\text{m}$ and the perception radius is equal to c. The $t_{\max}$ is set to the halfway between the lower and upper bound defined in Eq.(4.19), and the $\Delta t_{\text{samp}} = 0.25\,\text{s}$.

The results show that If the group of green people does not exist, the red pedestrian in all methods will overtakes the yellow on the right-handed side, but when the green exists, the red pedestrian in the social force model, the PLEdestrians, and the counterflow model still tries to overtake the yellow on the right-handed side and eventually get into trouble among the green people. This is because in the

social force and PLEdestrians, the desired velocity was fixed, which always points to the one end of the corridor, and the resulting walking direction was computed based on the simple actions like walking right when someone being left, which produces the awkward results as shown in Figure 7(b) and Figure 7(c). Although in the counterflow model the desired velocity was recomputed in every timestep, it was obtained in a greedy fashion by considering only the present states of the perceived people occupying in three overlapped front areas, and choosing a predefined walking direction towards a lowest-cost area. This still exhibits an awkward behavior as shown in Figure 7(d). In our MEM (Figure 7(e) and Figure 7(f)), the red pedestrian still tries to overtake the yellow on the right-handed side but when he perceives the green ones, he changes his direction to the left to reach more comfortable area.

The second scenario was shown in Figure 8. The red, blue, and yellow pedestrians are walking upward with desired speed 2.0 m/s, 1.3 m/s, and 0.5 m/s, respectively, and the green ones are walking downward with 1.3 m/s. The front line f, $t_{\max}$, and Δt_{samp} for the red pedestrian are identical to the previous scenario except that $c = 10\,\text{m}$. The results show that with the social force model (Figure 8(b)) the red pedestrian walked straight towards the group of green people and then was pushed back before escaping to the left, whereas with the PLEdestrians (Figure 8(c)) and the counterflow model (Figure 8(d)), the red pedestrian immediately turned his walking direction to the left when he perceived the green but he afterwards got stuck between the two slow yellow pedestrians. This was due to the opposed influences produced by each yellow pedestrian. If perceiving the people in back is allowed, the two yellow pedestrians will either be pushed or sidestep so that the red one can walk through, which should not be occurred since the adjacent lanes/areas are available.

With our MEM, the red pedestrian walks to the left to avoid the incoming green people, and then overtakes the yellow on the left and finally the blue people

on the right, as shown in Figure 8(e) and Figure 8(f). In case the desired speed of the red pedestrian decreases from 2.0 m/s to 1.3 m/s, he still avoids the incoming green

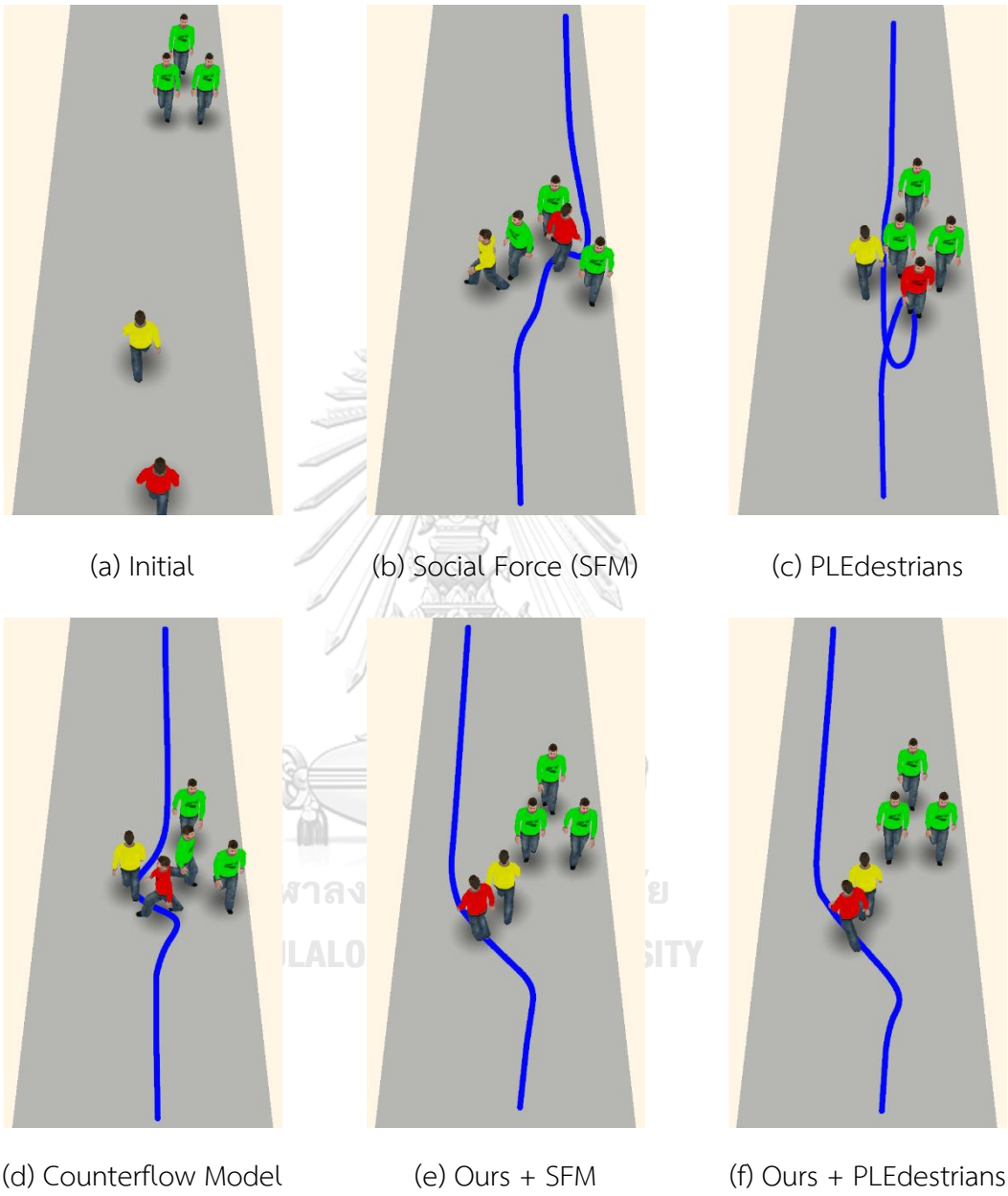

(a) Initial (b) Social Force (SFM) (c) PLEdestrians

(d) Counterflow Model (e) Ours + SFM (f) Ours + PLEdestrians

Figure 7. First-scenario comparison between our method and the other traditional ones.

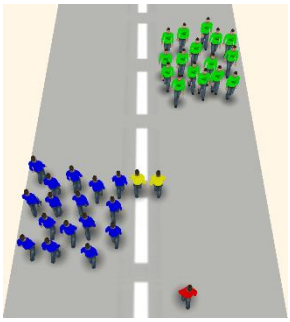

(a) Initial

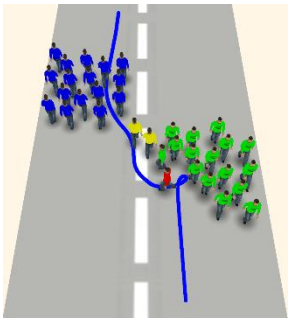

(b) Social Force (SFM)

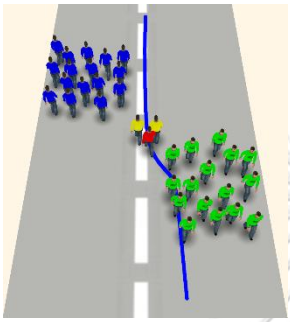

(c) PLEdestrians

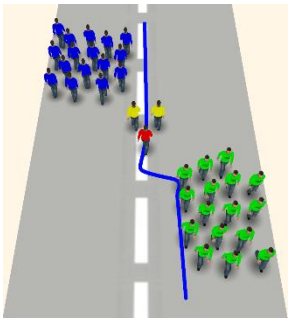

(d) Counterflow Model

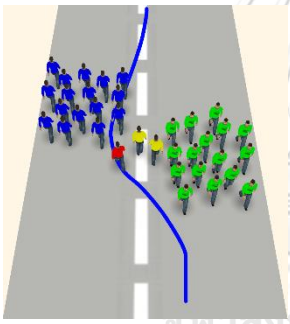

(e) Ours + SFM

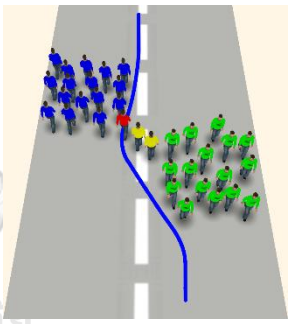

(f) Ours + PLEdestrians (2.0 m/s)

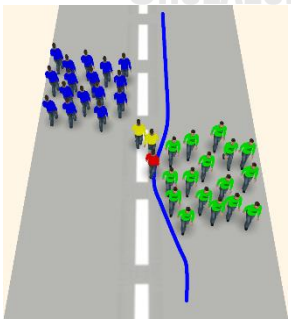

(g) Ours + PLEdestrians (1.3 m/s)

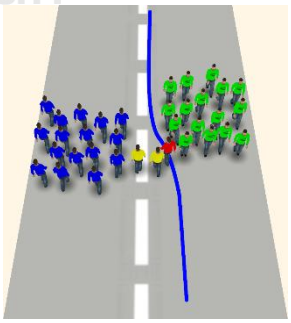

(h) Ours + PLEdestrians (3 m/s)

Figure 8. Second-scenario comparison between our method and the other traditional ones.

จุฬาลงกรณ์มหาวิทยาลัย
Chulalongkorn University

people in the same direction as before, but this time he chooses to overtake the yellow on the right, as shown in Figure 8(g), because this path is collision-free, shortest, and energy-minimal for the desired speed 1.3 m/s. On the other hand, when the desired speed increases to 3.0 m/s, he walks straight towards the incoming green people and passes through the crowds via a collision-free gap as shown in Figure 8(h). These behavioral varieties reflect the intelligence in his navigation.

5.2 Mimicking the Real-World Bidirectional Flow

We also mimicked the real-world bidirectional crowd flow by using our MEM along with the PLEdestrians for LCA, as shown in Figure 9 where the top rows show the image sequence from the video footage of bidirectional crowd flow, and the bottom rows show our mimicking results. Each simulated pedestrian has its own front line f with different planning distance c, and the $t_{\max}$ and Δt_{samp} are identical to the previous scenarios. After setting and tuning for c, the simulated pedestrians performed in the same manner as ones in the captured video, which can be seen from the movement of the rectangle-marked pedestrian in Figure 9(a) who runs fast in an upward direction (left column), then slows down for the expected gap (middle column), and finally accelerates to overtake the front people (right column), as well as the movement of the marked pedestrian in Figure 9(b) who walked fast (left column), then overtakes the people in front on the right (middle column), and finally goes through the crowd to the left (right column).

5.3 Lane Formation

One important phenomenon that inherently occurs in bidirectional crowd flow is lane formation. We conduct the experiment to observe this capability in our approach by placing a group of approximately one hundred pedestrians at each one end of the 13-meter-width corridor. The simulated pedestrians are placed randomly

in the group and prefer to walk to the opposite side at the desired speed 1.3 m/s. The planning distance c and the perception radius are set to 6 meters for all

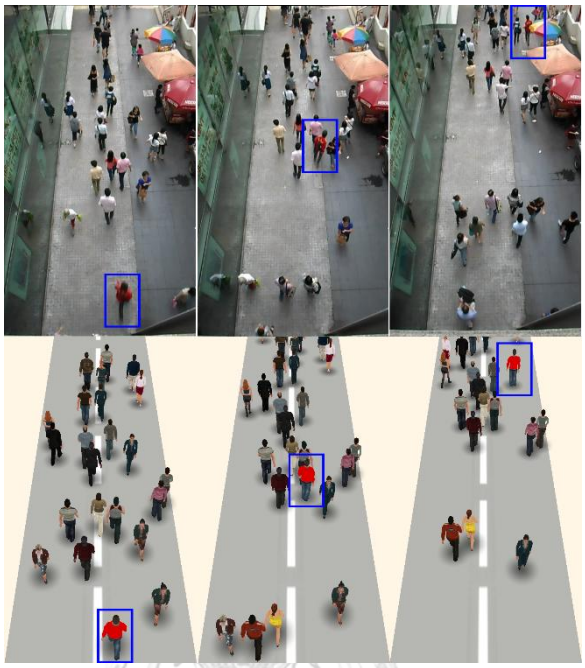

(a)

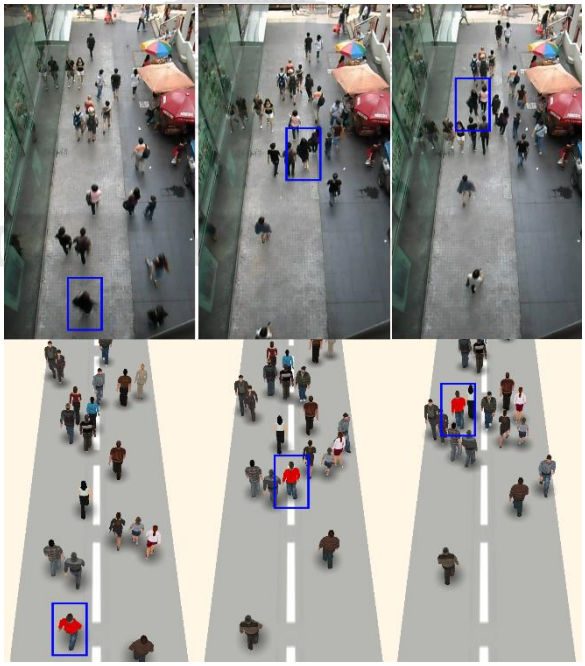

(b)

Figure 9. Mimicking the real-world bidirectional crowd flows.

pedestrians. The simulation result shows that after two groups meet each other around the middle of the corridor, the simulated pedestrians form 7 lanes as shown in Figure 10. If we use longer planning distance c, the lanes are formed faster. The lane formation was made in order to decrease the overall walking energy of the pedestrians, because following the people in front to reach the front line produces lower energy than facing the incoming people.

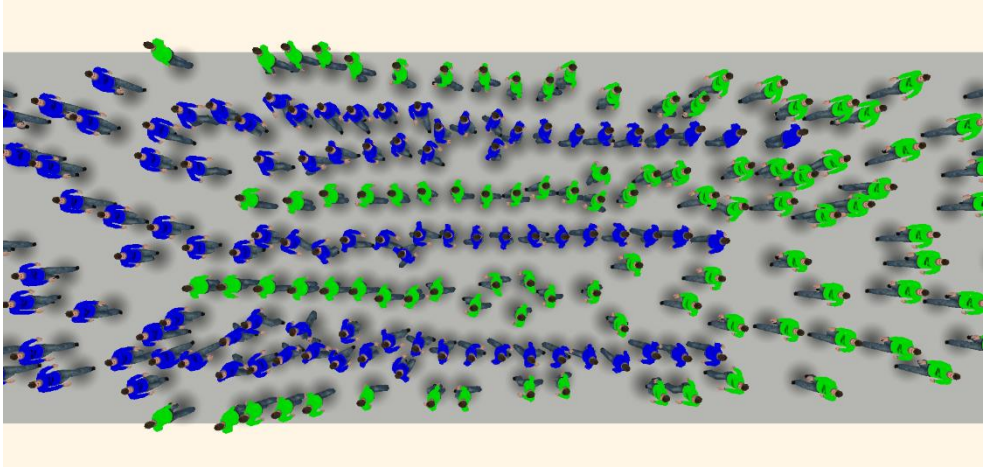

Figure 10. Lane formation simulation from a group of approximately one hundred pedestrians at each one end of the 13-meter-width corridor. The simulated pedestrians are placed randomly in the group and prefer to walk to the opposite side at the desired speed 1.3 m/s.

จุฬาลงกรณ์มหาวิทยาลัย
Chulalongkorn University

5.4 Fundamental Diagrams of Traffic Flow

We also quantitatively examine our approach in bidirectional crowd flows through the fundamental diagrams. The simulated pedestrians with the desired speed in a range from 1.3 m/s to 1.7 m/s are placed randomly in the 3m-wide and 15m-long corridor. The number of the pedestrians walking towards the right end of the corridor is equal to one towards the left end. If a pedestrian reaches to the one end, he will show up at the opposite and starts walking again. The $t_{\max}$ is set to be halfway between the lower and the upper bound defined in Eq.(4.19), $\Delta t_{\text{samp}} = 0.25\,\text{s}$, and the planning distance c is 3.66 m for all pedestrians. To

obtain the fundamental diagrams, we measure the average speed $\overline{v}$ and crowd density ρ in three areas locating at the middle and the ends of the corridor. Given $\overline{v}$ and ρ, the specific flow J_s is computed by using hydrodynamic relation $J_s = \rho\overline{v}$.

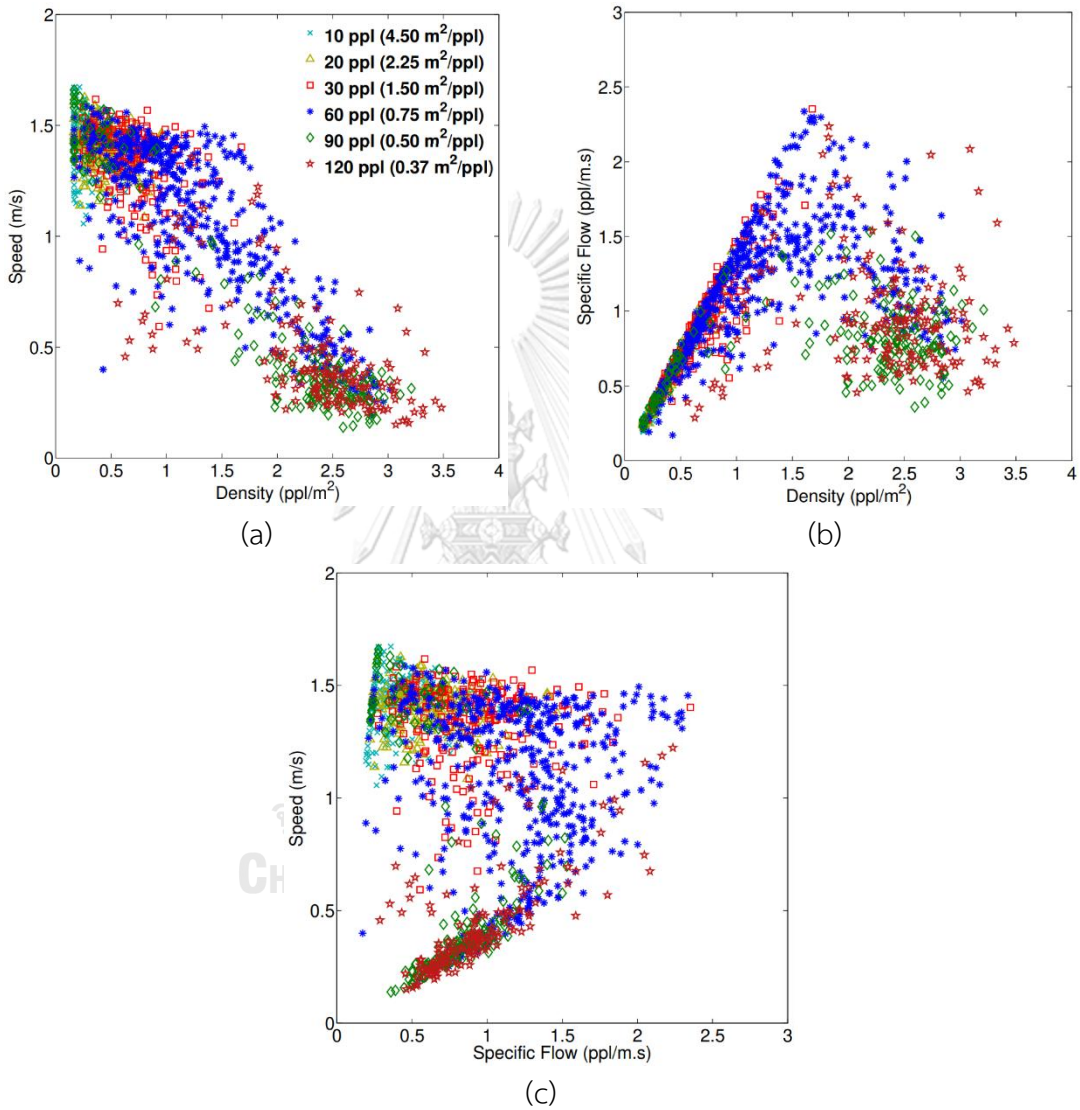

Figure 11. The fundamental diagrams of bidirectional crowd flows generated by our approach.

The flow will be examined at different numbers of pedestrians ranging from 10 to 120 people (equivalently to 0.37 m^2 to 4.50 m^2 maximum occupation area for a single pedestrian). The crowd density and the average speed in each area will

be measured every frame and averaged over a second interval. After running the simulation, the fundamental diagrams are obtained as shown in Figure 11. Notice that in case of 10 people (4.50 m^2/ppl) and 20 people (2.25 m^2/ppl), the walking speed of the pedestrians clings around the desired speed (1.3 m/s - 1.7 m/s) throughout the simulation time, but in case of 30 people (1.50 m^2/ppl) it sometimes a bit decreases due to higher population. When the number of pedestrians increases to 60, or the maximum occupation area per pedestrian reduces to 0.75 m^2, the walking speeds spread widely over the range from approximately 0.3 m/s to 1.6 m/s in a linearly-decreasing pattern as the density increases. This distribution results from dissolving the congestion into the free flow lanes. However, in a highly-dense crowd as demonstrated by the cases of 90 people (0.50 m^2/ppl) and 120 people (0.37 m^2/ppl), the free flow lanes are hardly constructed, which makes the pedestrians walk most of the time at the speeds ranging from approximately 0.15 m/s to 0.5 m/s. Given the specific flow, the relationship between the specific flow and the crowd density is shown in Figure 11(b), while the specific flow and the average speed shown in Figure 11(c). These diagrams have similar trend to the empirical data of bidirectional crowd flow [60] and the traffic flow theory [61].

5.5 Computation Time

จุฬาลงกรณ์มหาวิทยาลัย
CHULALONGKORN UNIVERSITY

The number of critical points, which depends on the user-defined parameters and the number of the perceived pedestrians, obviously has a great impact on the overall simulation time. To show the trend of the computation time on our approach, we measure the average time consumption in the situation when the pedestrians are randomly populated with different densities over the 3m-wide and 15m-long corridor. The desired speed for each pedestrian is randomly set in a range from 1.3 m/s to 1.7 m/s. At a certain population density, three different setting for the user-defined parameters: (1) $c = 3.66$ m, $\Delta t_{\text{samp}} = 0.25$ s, (2) $c = 3.66$ m, $\Delta t_{\text{samp}} = 0.50$ s, and (3) $c = 5.00$ m, $\Delta t_{\text{samp}} = 0.25$ s, will be used for the quantitative comparison.

After measuring at 12 population densities ranging from 0.2 ppl/m^2 to 2.66 ppl/m^2, the trend of the average computation times has been produced as shown in Figure 12. It is not surprising that at a certain population density the average computation time increases as the planning distance c increases and/or the sampling time Δt_{samp} decreases because the increase of c and/or the decrease of Δt_{samp} cause the higher number of critical points. However, when observing their margins, the average computation times in all three settings are not significantly different at the population densities below 1 ppl/m^2, but dramatically expand at the higher population densities. If the long planning distance c with the precise time sampling Δt_{samp} is used, the computation time must be expensive in high-density crowds. This is the limitation of our approach if the real-time computation for the dense crowds is required.

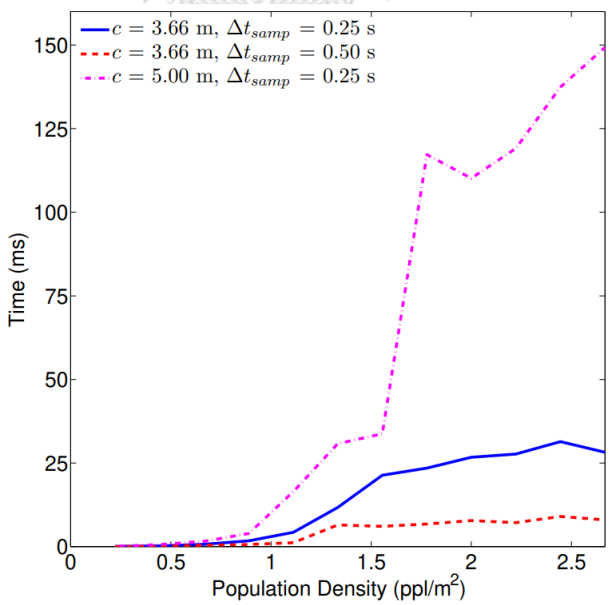

Figure 12. The average computation time of our approach in three different setting at different population densities.

5.6 Multi-Directional Crowd Flow

Our approach can be used in multi-directional crowd flow with a little modification. In bidirectional crowd flow, the pedestrian i is desired to walk towards the front line f but in multi-directional case the pedestrian i is desired to walk towards a circle with the radius specified by the user. The circle is centered at the pedestrian i's goal position. Figure 13 shows our simulation result in the scenario when two pedestrians try to walk across a flow of crowds. Pedestrians in the flow walk to the right with the same speed 1.3 m/s while two red pedestrians would like to walk to their own goals which located in the other side of the flow. Red pedestrian has a desired speed 2.0 m/s. The result shows that the red pedestrians can pass through the flow via the two tunnels that are marked with the red-colored rectangles.

In the other example as shown in Figure 14, pedestrians with the desired speeds ranging from 1.0 m/s to 1.4 m/s are placed at two circle boundaries (Figure 14(a)), and the goal position for each pedestrian is located at the opposite. At frame 725 (~12 seconds), the pedestrians in the social force model (Figure 14(b)), PLEdestrians (Figure 14(c)), and ORCA (Figure 14(d)) are mostly packed at the center, but when equipped with our MEM, the pedestrians are scattered and some of them almost reach to their own goal positions. This is because the pedestrians with our MEM respond to the others in an early time of simulation by planning the collision-free, comfortable paths towards their goals.

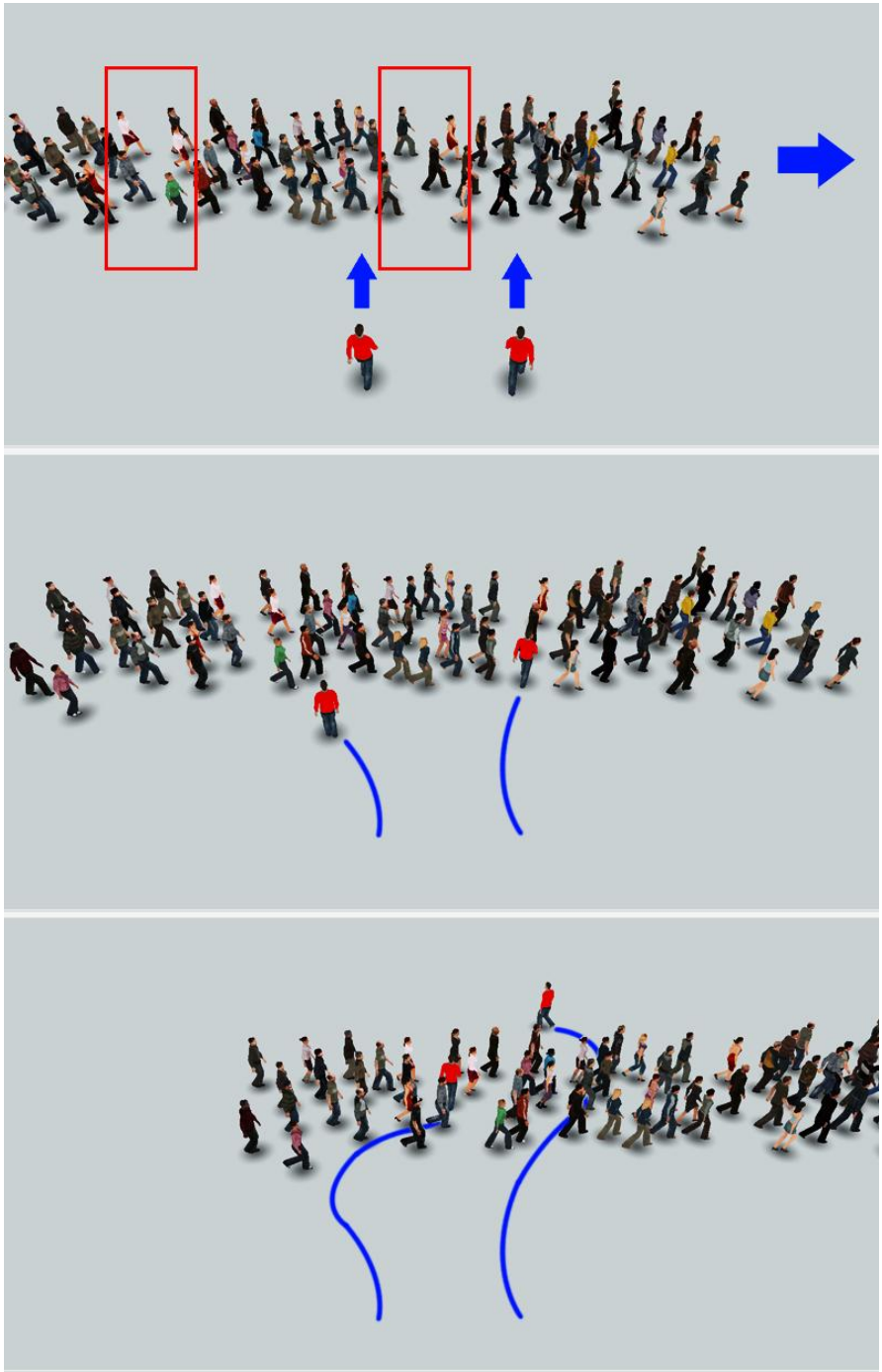

Figure 13. Image sequence (from top to bottom) of two red pedestrians walking upward against a flow of crowds by using our approach. The red pedestrians can walk through the flow via the two tunnels marked by the red-colored rectangles.

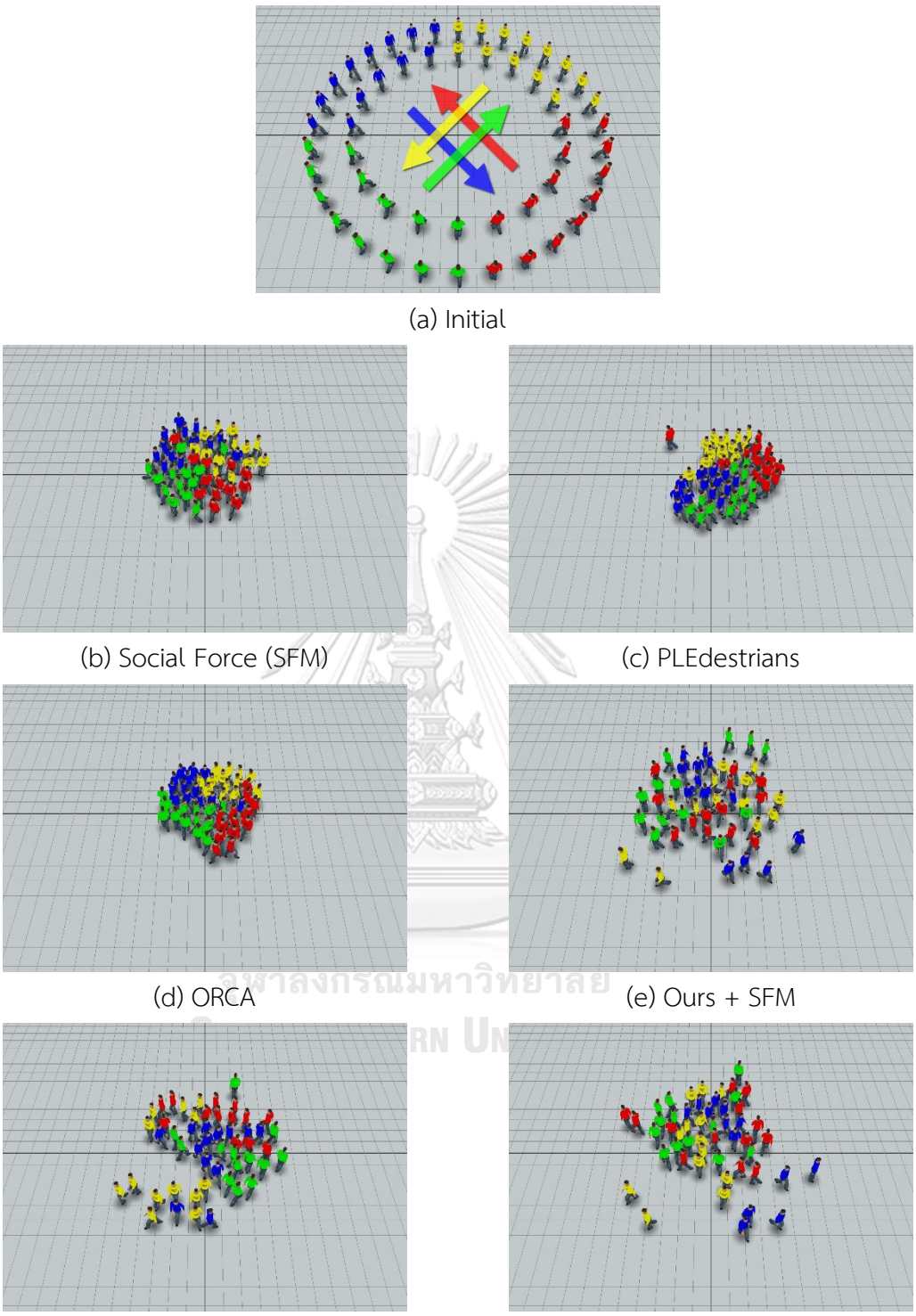

Figure 14. Comparison between our method and the other traditional ones in multi-directional crowd simulation.

CHAPTER 6
CONCLUSION AND FUTURE WORK

The short-term path planning based on the principle of least effort with the energy calculation using the metabolic energy equation of the real human walking was proposed. The technique can be seamlessly integrated with previous local collision avoidance methods, which allows the virtual pedestrians in bidirectional crowd flows to walk on energy-minimal paths. This results in more promising overtaking behavior and more reasonable lane changing direction, and in addition can achieve lane formation phenomenon and also generate the same trend of the fundamental diagrams as ones in the empirical data and the traffic flow theory. To obtain energy-minimal paths, we formulate the problem as the optimization problem and employ the optimal control theory with the dynamic programming as a solver. The algorithm can perform well in low-to-medium population density but yields the expensive computation in dense crowds. Also, our approach can be used for multi-directional crowd simulation with a little modification. For the future work, we plan to reduce the computational burden by finding the heuristic to determine when our MEM should operate, and the efficient method for adaptive planning distance c.

จุฬาลงกรณ์มหาวิทยาลัย
CHULALONGKORN UNIVERSITY

REFERENCES

1. Reynolds, C.W., *Flocks, Herds and Schools: A Distributed Behavioral Model.* SIGGRAPH Comput. Graph., 1987. **21**(4): p. 25-34.
2. LaValle, S.M., *Planning Algorithms*. 2006, New York, NY, USA: Cambridge University Press.
3. Shao, W. and D. Terzopoulos. *Environmental Modeling for Autonomous Virtual Pedestrians*. in *SAE Symposium on Digital Human Modeling for Design and Engineering*. 2005.
4. Botea, A., M. Müller, and J. Schaeffer, *Near optimal hierarchical path-finding.* Journal of Game Development, 2004. **1**: p. 7-28.
5. Kring, A.W., A.J. Champandard, and N. Samarin. *DHPA* and SHPA*: Efficient Hierarchical Pathfinding in Dynamic and Static Game Worlds*. in *AIIDE*. 2010. The AAAI Press.
6. Rantanen, M.T. and M. Juhola, *Using probabilistic roadmaps in changing environments.* Computer Animation and Virtual Worlds, 2014. **25**(1): p. 17-31.
7. Lamarche, F. and S. Donikian, *Crowd of Virtual Humans: a New Approach for Real Time Navigation in Complex and Structured Environments.* Computer Graphics Forum, 2004. **23**(3): p. 509-518.
8. Pettré, J., et al., *Real-time navigating crowds: scalable simulation and rendering.* Computer Animation and Virtual Worlds, 2006. **17**(3-4): p. 445-455.
9. Sud, A., et al. *Real-time Navigation of Independent Agents Using Adaptive Roadmaps*. in *Proceedings of the 2007 ACM Symposium on Virtual Reality Software and Technology*. 2007. New York, NY, USA: ACM.
10. Sud, A., et al. *Real-time Path Planning for Virtual Agents in Dynamic Environments*. in *ACM SIGGRAPH 2008 Classes*. 2008. New York, NY, USA: ACM.
11. Geraerts, R. and M.H. Overmars, *The Corridor Map Method: A General Framework for Real-time High-quality Path Planning: Research Articles.* Comput. Animat. Virtual Worlds, 2007. **18**(2): p. 107-119.
12. Karamouzas, I., R. Geraerts, and M. Overmars. *Indicative Routes for Path*

จุฬาลงกรณ์มหาวิทยาลัย
Chulalongkorn University

Planning and Crowd Simulation. in *Proceedings of the 4th International Conference on Foundations of Digital Games*. 2009. New York, NY, USA: ACM.

13. van Toll, W.G., A.F. Cook, and R. Geraerts, *A Navigation Mesh for Dynamic Environments.* Comput. Animat. Virtual Worlds, 2012. **23**(6): p. 535-546.
14. Jaklin, N., A.F.C. IV, and R. Geraerts, *Real-time path planning in heterogeneous environments.* Journal of Visualization and Computer Animation, 2013. **24**(3-4): p. 285-295.
15. Kumar, A. and A. Ojha, *Natural path planning using wavelet noise in static environment.* Computer Animation and Virtual Worlds, 2013. **24**(1): p. 17-24.
16. van Toll, W.G., I.A.F. Cook, and R. Geraerts, *Real-time Density-based Crowd Simulation.* Comput. Animat. Virtual Worlds, 2012. **23**(1): p. 59-69.
17. Sarmady, S., F. Haron, and A.Z. Talib, *Simulating Crowd Movements Using Fine Grid Cellular Automata.* 12th International Conference on Computer Modeling and Simulation, 2010. **0**: p. 428-433.
18. Bandini, S., et al. *A Cellular Automata Based Model for Pedestrian and Group Dynamics: Motivations and First Experiments*. in *Parallel Computing Technologies*. 2011. Springer Berlin Heidelberg.
19. Tajima, Y., K. Takimoto, and T. Nagatani, *Pattern formation and jamming transition in pedestrian counter flow.* Physica A: Statistical Mechanics and its Applications, 2002. **313**(3–4): p. 709-723.
20. Isobe, M., T. Adachi, and T. Nagatani, *Experiment and simulation of pedestrian counter flow.* Physica A: Statistical Mechanics and its Applications, 2004. **336**(3–4): p. 638-650.
21. Helbing, D. and P. Molnár, *Social force model for pedestrian dynamics.* Phys. Rev. E, 1995. **51**(5): p. 4282-4286.
22. Helbing, D., I. Farkas, and T. Vicsek, *Simulating dynamical features of escape panic.* Nature, 2000. **407**: p. 487-490.
23. Pelechano, N., J.M. Allbeck, and N.I. Badler. *Controlling Individual Agents in High-density Crowd Simulation*. in *Proceedings of the 2007 ACM SIGGRAPH/Eurographics Symposium on Computer Animation*. 2007. Aire-la-Ville, Switzerland, Switzerland: Eurographics Association.

จุฬาลงกรณ์มหาวิทยาลัย
Chulalongkorn University

24. Reynolds, C.W. *Steering Behaviors For Autonomous Characters*. in *the proceedings of Game Developers Conference 1999*. 1999.

25. Hartman, C. and B. Benes, *Autonomous Boids.* Comput. Animat. Virtual Worlds, 2006. **17**(3-4): p. 199-206.

26. Shao, W. and D. Terzopoulos, *Autonomous Pedestrians.* Graph. Models, 2007. **69**(5-6): p. 246-274.

27. Ond?ej, J., et al., *A Synthetic-vision Based Steering Approach for Crowd Simulation.* ACM Trans. Graph., 2010. **29**(4): p. 123-1.

28. Rymill, S.J. and N.A. Dodgson. *A Psychologically-Based Simulation of Human Behaviour*. in *EG UK Theory and Practice of Computer Graphics*. 2005. The Eurographics Association.

29. Guy, S.J., et al. *Simulating Heterogeneous Crowd Behaviors Using Personality Trait Theory*. in *Proceedings of the 2011 ACM SIGGRAPH/Eurographics Symposium on Computer Animation*. 2011. New York, NY, USA: ACM.

30. Fischer, L.G., R. Silveira, and L. Nedel. *GPU Accelerated Path-Planning for Multi-agents in Virtual Environments*. in *Games and Digital Entertainment (SBGAMES), 2009 VIII Brazilian Symposium on*. 2009.

31. Kapadia, M., et al. *Egocentric Affordance Fields in Pedestrian Steering*. in *Proceedings of the 2009 Symposium on Interactive 3D Graphics and Games*. 2009. New York, NY, USA: ACM.

32. Lerner, A., Y. Chrysanthou, and D. Lischinski, *Crowds by Example.* Computer Graphics Forum, 2007. **26**(3): p. 655-664.

33. Musse, S.R., et al., *Using Computer Vision to Simulate the Motion of Virtual Agents: Research Articles.* Comput. Animat. Virtual Worlds, 2007. **18**(2): p. 83-93.

34. Lerner, A., et al. *Fitting Behaviors to Pedestrian Simulations*. in *Proceedings of the 2009 ACM SIGGRAPH/Eurographics Symposium on Computer Animation*. 2009. New York, NY, USA: ACM.

35. Sun, L., X. Li, and W. Qin, *Simulating realistic crowd based on agent trajectories.* Computer Animation and Virtual Worlds, 2013. **24**(3-4): p. 165-172.

36. Paris, S., J. Pettré, and S. Donikian, *Pedestrian Reactive Navigation for Crowd Simulation: a Predictive Approach.* Computer Graphics Forum, 2007. **26**(3): p.

จุฬาลงกรณ์มหาวิทยาลัย
Chulalongkorn University

665-674.

37. Pettré, J., et al. *Experiment-based Modeling, Simulation and Validation of Interactions Between Virtual Walkers*. in *Proceedings of the 2009 ACM SIGGRAPH/Eurographics Symposium on Computer Animation*. 2009. New York, NY, USA: ACM.

38. Fiorini, P. and Z. Shillert, *Motion Planning in Dynamic Environments using Velocity Obstacles.* International Journal of Robotics Research, 1998. **17**: p. 760-772.

39. van den Berg, J., M. Lin, and D. Manocha. *Reciprocal velocity obstacles for real-time multi-agent navigation*. in *Proceedings - IEEE International Conference on Robotics and Automation*. 2008.

40. van den Berg, J., et al. *Interactive Navigation of Multiple Agents in Crowded Environments*. in *Proceedings of the 2008 Symposium on Interactive 3D Graphics and Games*. 2008. New York, NY, USA: ACM.

41. Guy, S.J., et al. *ClearPath: Highly Parallel Collision Avoidance for Multi-agent Simulation*. in *Proceedings of the 2009 ACM SIGGRAPH/Eurographics Symposium on Computer Animation*. 2009. New York, NY, USA: ACM.

42. van den Berg, J., et al. *Reciprocal n-Body Collision Avoidance*. in *ISRR*. 2009. Springer.

43. Guy, S.J., et al. *PLEdestrians: A Least-effort Approach to Crowd Simulation*. in *Proceedings of the 2010 ACM SIGGRAPH/Eurographics Symposium on Computer Animation*. 2010. Aire-la-Ville, Switzerland, Switzerland: Eurographics Association.

44. Golas, A., R. Narain, and M. Lin. *Hybrid Long-range Collision Avoidance for Crowd Simulation*. in *Proceedings of the ACM SIGGRAPH Symposium on Interactive 3D Graphics and Games*. 2013. New York, NY, USA: ACM.

45. Kim, S., S.J. Guy, and D. Manocha. *Velocity-based Modeling of Physical Interactions in Multi-agent Simulations*. in *Proceedings of the 12th ACM SIGGRAPH/Eurographics Symposium on Computer Animation*. 2013. New York, NY, USA: ACM.

46. Simo Kanmeugne, P. and A. Beynier. *Simulating Autonomous Pedestrians Navigation : A Generic Multi-Agent Model to Couple Individual and Collective*

จุฬาลงกรณ์มหาวิทยาลัย
Chulalongkorn University

Dynamics. in *Eighth International Workshop on Agents in Traffic and Transportation (ATT 2014)*. 2014. Paris, France.

47. Blue, V.J. and J.L. Adler, *Cellular automata microsimulation for modeling bi-directional pedestrian walkways.* Transportation Research Part B: Methodological, 2001. **35**(3): p. 293-312.
48. Xiang, L. and L.-Y. Dong, *Modeling and Simulation of Pedestrian Counter Flow on a Crosswalk.* Chinese Physics Letters, 2012. **29**(9): p. 9-13.
49. González, J., M.L. Sandoval, and J. Delgado, *Social Field Model to Simulate Bidirectional Pedestrian Flow Using Cellular Automata*, in *Traffic and Granular Flow ?11*, V.V. Kozlov, et al., Editors. 2013, Springer Berlin Heidelberg. p. 197-206.
50. Heliövaara, S., et al., *Counterflow model for agent-based simulation of crowd dynamics.* Building and Environment, 2012. **48**: p. 89-100.
51. Yuen, J.K.K. and E.W.M. Lee, *The effect of overtaking behavior on unidirectional pedestrian flow.* Safety Science, 2012. **50**(8): p. 1704-1714.
52. Ji, X., X. Zhou, and B. Ran, *A cell-based study on pedestrian acceleration and overtaking in a transfer station corridor.* Physica A: Statistical Mechanics and its Applications, 2013. **392**(8): p. 1828-1839.
53. Bruneau, J. and J. Pettré. *Energy-efficient Mid-term Strategies for Collision Avoidance in Crowd Simulation*. in *Proceedings of the 14th ACM SIGGRAPH / Eurographics Symposium on Computer Animation*. 2015. New York, NY, USA: ACM.
54. Zipf, G.K., *Human Behavior and the Principle of Least Effort*. 1949: Addison-Wesley.
55. Richards, J., *Biomechanics in clinic and research: an interactive teaching and learning resource*. 2008: Churchill Livingstone.
56. Seierstad, A. and K. Sydsæter, *Optimal Control Theory with Economic Applications*. 1987: Elsevier Science.
57. Kamien, M.I. and N.L. Schwartz, *Dynamic Optimization: The Calculus of Variations and Optimal Control in Economics and Management (Advanced Textbooks in Economics)*. 1991: Elsevier Science; 2nd edition (October 25, 1991).

58. Kirk, D.E., *Optimal Control Theory: An Introduction*. Dover Books on Electrical Engineering Series. 2004: Dover Publications.

59. Hall, E.T., *The Hidden Dimension*. A Doubleday anchor book. 1990: Anchor Books.

60. Zhang, J., et al., *Ordering in bidirectional pedestrian flows and its influence on the fundamental diagram.* Journal of Statistical Mechanics: Theory and Experiment, 2012. **2**: p. 02002.

61. Kachroo, P.P.E., et al., *Pedestrian Dynamics*. 2008: Springer Berlin Heidelberg.

จุฬาลงกรณ์มหาวิทยาลัย
CHULALONGKORN UNIVERSITY

จุฬาลงกรณ์มหาวิทยาลัย
Chulalongkorn University

VITA

NAME	Saran Sillapaphiromsuk
DATE OF BIRTH	27 November 1986
PLACE OF BIRTH	Lampang

จุฬาลงกรณ์มหาวิทยาลัย
CHULALONGKORN UNIVERSITY